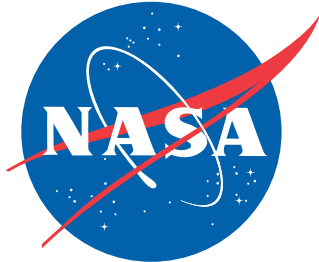# DDFRG2: Double-Differential FRaGmentation Model with Pion Production

John W. Norbury
Langley Research Center, Hampton, Virginia

January 2023

NASA STI Program Report Series

Since its founding, NASA has been dedicated to the advancement of aeronautics and space science. The NASA scientific and technical information (STI) program plays a key part in helping NASA maintain this important role.

The NASA STI program operates under the auspices of the Agency Chief Information Officer. It collects, organizes, provides for archiving, and disseminates NASA's STI. The NASA STI program provides access to the NTRS Registered and its public interface, the NASA Technical Reports Server, thus providing one of the largest collections of aeronautical and space science STI in the world. Results are published in both non-NASA channels and by NASA in the NASA STI Report Series, which includes the following report types:

- TECHNICAL PUBLICATION. Reports of completed research or a major significant phase of research that present the results of NASA Programs and include extensive data or theoretical analysis. Includes compilations of significant scientific and technical data and information deemed to be of continuing reference value. NASA counterpart of peer-reviewed formal professional papers but has less stringent limitations on manuscript length and extent of graphic presentations.

- TECHNICAL MEMORANDUM. Scientific and technical findings that are preliminary or of specialized interest, e.g., quick release reports, working papers, and bibliographies that contain minimal annotation. Does not contain extensive analysis.

- CONTRACTOR REPORT. Scientific and technical findings by NASA-sponsored contractors and grantees.

- CONFERENCE PUBLICATION. Collected papers from scientific and technical conferences, symposia, seminars, or other meetings sponsored or co-sponsored by NASA.

- SPECIAL PUBLICATION. Scientific, technical, or historical information from NASA programs, projects, and missions, often concerned with subjects having substantial public interest.

- TECHNICAL TRANSLATION. English-language translations of foreign scientific and technical material pertinent to NASA's mission.

Specialized services also include organizing and publishing research results, distributing specialized research announcements and feeds, providing information desk and personal search support, and enabling data exchange services.

For more information about the NASA STI program, see the following:

- Access the NASA STI program home page at http://www.sti.nasa.gov

- Help desk contact information:

https://www.sti.nasa.gov/sti-contact-form/ and select the "General" help request type.

NASA/TP-20220016654
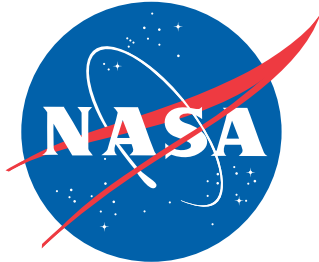
DDFRG2: Double-Differential FRaGmentation model with Pion Production

John W. Norbury
Langley Research Center, Hampton, Virginia

National Aeronautics and
Space Administration

Langley Research Center
Hampton, Virginia 23681-2199

January 2023

Acknowledgments

Contents

List of Tables

List of Figures

Nomenclature

A	Nucleus symbol
c	Speed of light (units throughout paper are such that $c \equiv 1$)
$\mathcal{C}$	Central fireball reference frame
dp^3	Momentum volume element, $dp^3 = p^2 dp d\Omega$
eV	Electron volt
E	Total energy, $E = T + m$ (sum of kinetic energy and rest-mass energy)
$E_{\pi\mathcal{C}}$	Total pion energy in the central fireball frame
$E_{\pi L}$	Total pion energy in the lab frame
$F(\theta)$	Correction factor
$f(x)$	Generic function of arbitrary variable, x
$g(x)$	Generic function of arbitrary variable, x
$h(x)$	Generic function of arbitrary variable, x
GeV	Giga electron volt (10^9 eV)
K_1	Modified Bessel function of the second kind
L	Laboratory (lab) reference frame (same as target frame, assuming a stationary target)
m	Mass
m_N	Nucleon mass
m_{p}	Proton mass
m_π	Pion mass
mb	millibarn
MeV	Mega electron volt (10^6 eV)
GeV	Giga electron volt (10^9 eV)
N	Nucleon symbol
$\mathcal{N}$	Normalization constant
$\mathcal{N}'(\theta)$	Modified normalization constant, $\mathcal{N}'(\theta) \equiv F(\theta)\,\mathcal{N}$
p	Proton symbol
$\mathbf{p}$	3-momentum vector
p	Magnitude of 3-momentum vector $p \equiv |\mathbf{p}|$
p_{break}	Momentum break point
$p_{\pi\mathcal{C}}$	Pion 3-momentum in the central fireball frame
$p_{\pi L}$	Pion 3-momentum in the lab frame
$\mathcal{P}$	Projectile frame
T	Kinetic energy
T_{break}	Kinetic energy break point
$T_{\pi\mathcal{C}}$	Pion kinetic energy in the central fireball frame
$T_{\pi L}$	Pion kinetic energy in the lab frame
$T_{\mathcal{P}L}$	Kinetic energy of the projectile frame relative to the lab frame

T_p	Kinetic energy of proton projectile
z	$\cos\theta_{\pi L}$
Z	Charge of projectile
β	Speed, in units of c
$\beta_{\mathcal{C}L}$	Speed of the central fireball frame relative to the lab frame
γ	Relativistic factor $\gamma \equiv 1/\sqrt{1-\beta^2}$
$\gamma_{\mathcal{C}L}$	Relativistic factor of the central fireball frame relative to the lab frame
Ω	Solid angle
π	Pion symbol
σ	Total cross section
θ	Longitudinal angle
$\theta_{\pi\mathcal{C}}$	Pion emission angle in the central fireball frame
$\theta_{\pi L}$	Pion emission angle in the lab frame
Θ	Temperature
Θ_π	Temperature of the central fireball pion source
$\Theta_{\pi\,\text{break}}$	Temperature of the central fireball pion source after pion momentum break
$\frac{d\sigma}{dE}$	Single-differential spectral (energy) distribution cross section
$\frac{d\sigma}{d\Omega}$	Single-differential angular distribution cross section
$\frac{d^2\sigma}{dEd\Omega}$	Double-differential cross section
$E\frac{d^3\sigma}{dp^3}$	Lorentz-invariant double-differential cross section
$\forall$	Mathematical symbol "for all"

Abstract

A set of Double-Differential FRaGmentation (DDFRG) models for production of fragments from nucleon-nucleus and nucleus-nucleus collisions, relevant to space radiation, is currently being developed. DDFRG1 was a previous model developed for production of protons and light ions. A new model for pion production is developed in the present work and is called DDFRG2, which is based upon thermal production of pions from a central fireball source. The Lorentz-invariant double-differential cross section is calculated in the central fireball frame, and is Lorentz transformed to the laboratory frame, which results in a closed-form analytic formula involving no numerical integration, and which can be run very efficiently in radiation transport codes. The Lorentz-invariant double-differential cross section is then integrated over angle to give the single-differential energy spectral distribution. Two versions of the DDFRG2 pion production are developed, namely DDFRG2-SIMPLE and DDFRG2-FULL. Both versions produce pion production Lorentz-invariant double-differential cross sections and also pion production single-differential spectral (energy) distributions. The SIMPLE version contains only one adjustable parameter. The FULL version contains three additional adjustable parameters. Both DDFRG2 versions are compared to over 1,000 data points. The SIMPLE version describes the $p + {}^{12}C \rightarrow \pi^-$ much better than the current HZETRN pion model. For other reactions, the SIMPLE version is of comparable quality to the current HZETRN pion model compared to data. For both the $p + {}^{12}C \rightarrow \pi^-$ reaction and all other reactions, DDFRG2-FULL describes the data much more accurately than the current HZETRN pion model.

1 Introduction

The importance of pion contributions to absorbed dose in space radiation shielding studies was first illustrated by Aghara et al. [1], who showed that pion contributions to dose[1] could be as large as 20%. Recent modeling efforts, using space radiation transport codes, have demonstrated the crucial importance of including pion interactions for correct predictions of absorbed radiation dose compared to data collected on balloon flights [2, 3] and the International Space Station (ISS) [4]. Other hadrons, such as kaons, η, and ρ mesons may also need to be included [4] in future work.

Double-differential cross sections, as a function of the energy and angle of the produced fragment, are necessary for light mass fragments because they scatter at large angles. A Double-Differential FRaGmentation model, hereafter referred to as DDFRG1,

---

[1]This is the contribution to dose. The contribution to dose-equivalent is smaller.

1

has recently been developed [5, 6] to calculate double-differential cross sections for production of protons and light ions, i.e. isotopes of Hydrogen (H) and Helium (He) produced in galactic cosmic ray (GCR) interactions with target materials. Pions are also light in mass and scatter at large angles, requiring double-differential cross sections to be used in space radiation transport codes. The aim of the present work is to adapt the previously developed DDFRG1 model [5, 6] to include the production of pions, in addition to light ions. A new model, hereafter referred to as DDFRG2, will be the result.

The previously developed DDFRG1 model [5, 6] consisted of two parts. The first part was a double-differential cross section model for proton (^{1}H) production. This model was developed separately and validated against a comprehensive set of experimental data. The second part of DDFRG1 consisted of a double-differential cross section model for other light ions, namely ^{2}H, ^{3}He, ^{4}He. The light ion model was a coalescence model that used the proton production model as input. The first model for proton production is the piece that will be modified to develop the present pion production model.

The DDFRG1 model [5, 6] was rather complicated, in that both protons and light ions were produced from four separate sources, namely thermal production from the projectile frame, direct particle production from the projectile frame, thermal production from the target frame, and thermal production from the central fireball frame. The complications of having to deal with four sources will not be necessary for pion production, because it is well known that pion production needs a very hot, thermal environment, and this is only provided by the central fireball, which is the region where the projectile and target nuclei overlap during the collision process.

2 Pion cross section model

The pion production model for DDFRG2 will be much simpler than the DDFRG1 proton production model, because pions are predominantly produced in the very hot central fireball region. Therefore, only a single central fireball pion source is necessary. The Lorentz-invariant double-differential cross section thermal model for a single [5, 6] pion source is

$$E_{\pi\mathcal{C}}\frac{d^3\sigma_\pi}{dp^3_{\pi\mathcal{C}}}(p_{\pi C}, \theta_{\pi C}) = \mathcal{N}e^{-T_{\pi C}/\Theta_\pi}, \tag{1}$$

where $E_{\pi\mathcal{C}}$, $p_{\pi\mathcal{C}}$, $\theta_{\pi\mathcal{C}}$, and $T_{\pi\mathcal{C}}$ are the total pion energy, momentum, emission angle, and kinetic energy in the central fireball frame, $\mathcal{C}$. The momentum symbol, p, represents the magnitude of the 3-momentum, $p \equiv |\mathbf{p}|$. The temperature (in units of energy) of the central fireball pion source is Θ_π, and $\mathcal{N}$ is the cross section normalization ensuring that the integral of the Lorentz-invariant double-differential cross section is equal to the total cross section, σ. Transport codes [7, 8, 9, 10, 11] require cross sections evaluated in the lab frame, L, which is the spacecraft reference frame where astronauts are located.

Lorentz transforming equation (1) to the lab frame yields[2] the final form of the pion Lorentz-invariant differential cross section written in terms of lab frame variables,

$$E_{\pi L}\frac{d^3\sigma_\pi}{dp_{\pi L}^3}(p_{\pi L},\theta_{\pi L}) = \mathcal{N}\exp[(m_\pi - \gamma_{\mathcal{C}L}\sqrt{p_{\pi L}^2 + m_\pi^2} + \gamma_{\mathcal{C}L}\,\beta_{\mathcal{C}L}\,p_{\pi L}\cos\theta_{\pi L})/\Theta_\pi]\,, \quad (2)$$

where $E_{\pi L}$, $p_{\pi L}$, $\theta_{\pi L}$, and $T_{\pi L}$ are the total pion energy, momentum, emission angle, and kinetic energy in the lab frame[3], L. The pion mass is m_π. The temperature, Θ_π, is calculated using the simple analytic expression in reference [13]. The relativistic factors for the central frame, relative to the lab frame, are

$$\gamma_{\mathcal{C}L} \equiv \sqrt{1 + \frac{T_{\mathcal{P}L}}{2m_N}}\,, \qquad \beta_{\mathcal{C}L} = \sqrt{1 - \frac{1}{\gamma_{\mathcal{C}L}^2}}\,. \quad (3)$$

where m_N is the nucleon mass and $T_{\mathcal{P}L}$ is the kinetic energy[4] of the projectile frame, relative to the lab frame. The β factor is the speed in units of the speed of light, c.

2.1   Normalization

The calculation of the normalization for a single source is now reviewed. (*For ease of reading, the pion subscript, π, will not be shown explicitly in many equations that follow.*) The pion momentum volume element is $dp^3 = p^2 dp d\Omega$, where the solid angle is $d\Omega = 2\pi\sin\theta d\theta$, assuming azimuthal symmetry. The relativistic expressions relating the total energy, E, kinetic energy, T, mass, m, and 3-momentum, $\mathbf{p}$, of the emitted pion are the Einstein equations [12],

$$E \equiv T + m = \gamma m\,, \quad (4)$$

and

$$E^2 \equiv \mathbf{p}^2 + m^2\,, \quad (5)$$

with units where the speed of light is $c \equiv 1$, which is the standard convention used throughout this paper. In terms of speed, β, the relativistic γ factor[5] is $\gamma \equiv (1 - \beta^2)^{-\frac{1}{2}}$.

The general thermal model expression [5, 6] for the Lorentz-invariant double-differential cross section for production of a pion is

$$E\frac{d^3\sigma}{dp^3} = \mathcal{N}e^{-T/\Theta}\,, \quad (6)$$

---

[2]Lorentz transformations are discussed extensively in reference [12].
[3]Assuming that the target does not move, then the lab frame is identical to the target frame.
[4]In accelerator experiments, $T_{\mathcal{P}L}$ is often called the beam energy.
[5]The usual definition is $\beta \equiv v/c$, where v is speed. In units where $c \equiv 1$, then $\beta = v$.

where T is the kinetic energy of the emitted pion. The constant $\mathcal{N}$ is determined from the normalization requirement,

$$\sigma \equiv \int \frac{d^3p}{E} \, E \frac{d^3\sigma}{dp^3} = \int \frac{d^3p}{E} \, \mathcal{N} e^{-T/\Theta} \, , \tag{7}$$

with the 3-momentum integral given by

$$\int \frac{d^3p}{E} = 2\pi \int d\theta \sin\theta \int dT \sqrt{T(T+2m)} \, . \tag{8}$$

The final expression is

$$\sigma = \mathcal{N} \, 2\pi \int_{\theta_{\min}}^{\theta_{\max}} d\theta \sin\theta \int_{T_{\min}}^{T_{\max}} dT \sqrt{T(T+2m)} \, e^{-T/\Theta} \, , \tag{9}$$

or

$$\mathcal{N} = \frac{\sigma}{2\pi \int_{\theta_{\min}}^{\theta_{\max}} d\theta \sin\theta \int_{T_{\min}}^{T_{\max}} dT \sqrt{T(T+2m)} \, e^{-T/\Theta}} \, , \tag{10}$$

where integration limits for angle are written as $\theta_{\min}$, $\theta_{\max}$, and for kinetic energy, as $T_{\min}$, $T_{\max}$.

Combining equations (6) and (10) gives the most general form of the correctly normalized single source thermal model as

$$E\frac{d^3\sigma}{dp^3} = \left[\frac{\sigma}{2\pi \int_{\theta_{\min}}^{\theta_{\max}} d\theta \sin\theta \, \int_{T_{\min}}^{T_{\max}} dT \sqrt{T(T+2m)} \, e^{-T/\Theta}} \right] e^{-T/\Theta} \, , \tag{11}$$

which is in agreement[6] with Werneth et al. [13]. The term in the square brackets[7] in equation (11) is the normalization constant, $\mathcal{N}$.

2.1.1 Normalization of DDFRG1

In the DDFRG1 model [5, 6], the integration limits were chosen as[8]

$$\theta_{\min} = 0, \quad \theta_{\max} = \pi, \tag{12}$$

$$T_{\min} = 0, \quad T_{\max} = \infty. \tag{13}$$

---

[6]Equation (10) in reference [13] should not have 2π in the denominator.

[7]The term, $e^{-T/\Theta}$, in the denominator is part of the integrand and does not "cancel" out the term in the numerator.

[8]The maximum kinetic energy is, of course, a finite value determined by conservation of momentum. The ∞ upper limit is an approximation.

The choice of the integration limits in equations (12) and (13) allowed for simple, analytic, closed-form parameterizations, because of the following exact expressions for the integrals [14] in equation (11),

$$2\pi \int_0^\pi d\theta \sin\theta \;\; = \;\; 4\pi \;, \tag{14}$$

$$\int_0^\infty dT \sqrt{T(T+2m)} \, e^{-T/\Theta} \;\; = \;\; m\Theta e^{m/\Theta} K_1(m/\Theta) \;, \tag{15}$$

where $K_1(m/\Theta)$ is the modified Bessel function of the second kind [15] of order 1 as a function of m/Θ, giving the thermal model total cross section from equation (9) as

$$\sigma = 4\pi \mathcal{N} m\Theta e^{m/\Theta} K_1(m/\Theta) \;. \tag{16}$$

Substitution into equation (11) led to the simple, closed-form expression for the final thermal model [5, 6],

$$E\frac{d^3\sigma}{dp^3} = \frac{\sigma}{4\pi m\Theta K_1(m/\Theta)} \, e^{-(T+m)/\Theta} \;, \tag{17}$$

correctly normalized so that the integral of the Lorentz-invariant differential cross section gives the total cross section.

2.1.2 Normalization of DDFRG2

The same approximate integration limits in equations (12) and (13) will also be used for the present DDFRG2 pion production models, because they enable one to derive a closed-form analytic expression for the normalization factor, $\mathcal{N}$, and therefore, upon substitution into equation (2), enable a closed-form analytic expression to be derived for the Lorentz-invariant double-differential cross section. Because the integration limits are only approximate, a small multiplicative parameter, $F(\theta)$, is introduced as a correction factor. In the DDFRG2-SIMPLE model there is no such extra parameter, so that $F(\theta){=}1$. In the DDFRG2-FULL model, the values of $F(\theta)$ are obtained from Table 1. The normalization factor, $\mathcal{N}$, in equation (10) contains the total pion production cross section, σ, which is calculated according to the methods of reference [16]. The final expression for the pion production Lorentz-invariant differential cross section is given by equation (2), with $\mathcal{N}$ replaced by $\mathcal{N}'(\theta)$, given as

$$\boxed{\mathcal{N}'(\theta) \equiv F(\theta)\,\mathcal{N} = F(\theta)\,\frac{\sigma}{4\pi m\Theta K_1(m/\Theta)e^{m/\Theta}}}\;. \tag{18}$$

The value of σ is different for each of the charged pion species (π^+, π^-, π^0), resulting in a different value of $\mathcal{N}$ for each pion, and consequently a different value of the Lorentz-invariant differential cross section, $E_{\pi L}\frac{d^3\sigma_\pi}{dp_\pi^3}$, for each pion, as given by equation (2).

2.2 Negative pion production at forward angles from low energy proton-nucleus reactions

Inclusive negative pion production from proton-nucleus reactions is generically written

$$p + A \rightarrow \pi^- \tag{19}$$

Some data for the reaction $p + {}^{12}C \rightarrow \pi^-$ with low proton projectile energies of 1.05 GeV and 2.1 GeV, appear in Figure 1. The data show a sharp break point in the momentum spectrum near 1 GeV and 2 GeV respectively. Such a sharp break is unique to this reaction and does not appear in any of the other data in Figures 1 - 11. Why is this particular reaction unique?

The $p + {}^{12}C \rightarrow \pi^-$ reaction is unique for the following *combined* reasons:

1. The produced pions have a negative charge.

2. The pions are produced at a very small angle. The data in Figure 1 show pions produced at the very forward angle, $\theta_{\pi\,\text{lab}} = 0°$.

3. The proton projectile energy is not very large. The data in Figure 1 are obtained with proton projectile energies of 1.05 GeV and 2.1 GeV.

Protons of very high energy can travel directly through the nucleus before undergoing an interaction, and if an interaction does occur, then produced pions are sufficiently energetic to travel straight out of the nucleus. Low energy pions are produced by low energy protons and will undergo more scattering, but negative pions are especially prone to absorption before escaping the nucleus due to the nucleus containing many positively charged protons. The low energy negative pions are easily absorbed through spallation reactions, which are like a "mini-explosion" inside the nucleus due to the probability of large interactions between negatively charged pions and positively charged protons. Pions produced at very forward angles have a much larger distance to travel through the nucleus, compared to larger angle pions, and therefore absorption is more likely at small production angles.

Based on the above considerations, a theoretical model is now developed with the aim of reproducing the unique data shown in Figure 1, and also being sufficiently general to describe all reactions involving negative pion production at forward angles from low energy proton-nucleus collisions.

The experimental data clearly show a break in the spectrum at a specific momentum value which will be called, p_{break}. The temperature shows a significant drop above p_{break}. In order to model this, different thermal distribution functions will be required below and above the break point. For an arbitrary variable x, this is stated mathematically as

$$f(x) = g(x), \quad \forall \quad x < x_{\text{break}}, \tag{20}$$
$$f(x) = h(x), \quad \forall \quad x \geq x_{\text{break}}, \tag{21}$$

where the standard mathematical symbol, $\forall$, reads "for all". However, such a scheme will never work because, in general, two arbitrary functions will have completely different values at x_{break}. The two functions need to be forced to have the same value at the break point, which can be obtained by relating the second function to the first function (or vice-versa) with a normalization factor, as in

$$f(x) = g(x), \qquad\qquad \forall \quad x < x_{\text{break}}, \qquad\qquad (22)$$

$$f(x) = \frac{g(x_{\text{break}})}{h(x_{\text{break}})} h(x), \quad \forall \quad x \geq x_{\text{break}}. \qquad\qquad (23)$$

In the application in the present work, $g(x)$ and $h(x)$ simply represent two thermal distribution functions of the form of equation (6), with each function having a different temperature, Θ_1 and Θ_2, so that equation (6) is re-written as

$$E\frac{d^3\sigma}{dp^3} = \mathcal{N}'e^{-T/\Theta_1}, \qquad\qquad\qquad\qquad\qquad \forall \quad T < T_{\text{break}},$$

$$E\frac{d^3\sigma}{dp^3} = \mathcal{N}'\left(\frac{e^{-T_{\text{break}}/\Theta_1}}{e^{-T_{\text{break}}/\Theta_2}}\right) e^{-T/\Theta_2} = \mathcal{N}'e^{-T_{\text{break}}/\Theta_1} e^{(T_{\text{break}}-T)/\Theta_2}, \quad \forall \quad T \geq T_{\text{break}} .(24)$$

The modified thermal spectrum is only implemented for negative pion production from proton-nucleus reactions with pion emission lab angles smaller than a critical angle of $5°$, and pion lab momenta greater than $p_{\pi L\text{break}}$, where the pion momentum is calculated from equations (4) and (5) giving $p_{\pi L\text{break}} = \sqrt{T_{\text{break}}(2T_{\text{break}} + m_\pi)}$.

The *implementation* into the final equation (2) is as follows:

1. Use equation (2) for values of $p_{\pi L} < p_{\pi L\text{break}}$. The temperature, $\Theta_1 \equiv \Theta_\pi$, is calculated as usual from the simple expression in reference [13].

2. Use equation (2) for values of $p_{\pi L} \geq p_{\pi L\text{break}}$, but with the substitution $\mathcal{N} \rightarrow \mathcal{N}\left(\frac{e^{-T_{\text{break}}/\Theta_1}}{e^{-T_{\text{break}}/\Theta_2}}\right)$ and $\Theta_\pi \rightarrow \Theta_2$, parameterized in Table 2 as $\Theta_2 = 0.2 \times \Theta_1$.

2.2.1 Calculation of break point

The calculation of the actual numerical value of the break point is enabled by the hypothesis that the break point occurs at the maximum value of the outgoing pion momentum. The details of this calculation can be found in the Appendix of Section 6. The maximum value of the outgoing pion momentum and energy is evaluated in the center of momentum frame in Section 6.1. However, the data in Figures 1 - 2 are given in the lab frame, and so the maximum pion momentum and energy are Lorentz transformed to the lab frame in Section 6.2. The final equation (67) gives the maximum pion momentum in the lab

frame as

$$p_{\text{break}} = p_{\pi L \text{ max}} \equiv |\mathbf{p}_{\pi L \text{ max}}|$$

$$= \sqrt{\frac{1}{16m_N^2}\left[2m_N T_{\mathcal{P}L} + m_\pi^2 + \sqrt{\frac{T_{\mathcal{P}L}[m_\pi^4 - 4m_\pi^2 m_N T_{\mathcal{P}L} + 4m_N^2(T_{\mathcal{P}L}^2 - 4m_\pi^2)]}{T_{\mathcal{P}L} + 2m_N}}\right]^2 - m_\pi^2}.$$

(25)

Calculated break points are given in Table 3, and are seen to occur exactly where the experimental data shown in Figure 1 display a transition, or break, to a different temperature. This fully supports the hypothesis that the break points occur at the value of the maximum momentum of the outgoing pion. The reason that the data continue past the momentum break point is most likely due to Fermi motion. The success of the break point calculation also lends support to the previous comments concerning the uniqueness of the p + ^{12}C → π^- reaction at $T_{\mathcal{P}L}$ = 1.05 GeV, 2.1 GeV and $\theta_{\pi \text{ lab}} = 0°$, because no other experimental data shows similar break points.

2.3 Complete model

Equations (2) and (18) constitute the final form of the DDFRG2 model for the Lorentz-inavariant double-differential cross section that will be compared to experimental data in Figures 1 - 11. The FULL ($F(\theta)$ from Table 1) or SIMPLE ($F(\theta) \equiv 1$) versions are obtained depending on the values of $F(\theta)$. In Figures 1 - 11, the red solid curves (labelled DDFRG) use the FULL form of the normalization in equation (18), using the values of $F(\theta)$ given in Table 1. The green dashed curves (labelled SIMPLE) in Figures 1 - 11 use equation (18), but with no correction factor applied, namely $F(\theta) = 1$. A detailed discussion of models versus data can be found in Section 4. Sample results for the DDFRG2-FULL and DDFRG2-SIMPLE models are listed in Tables 4 and 5 respectively.

3 Differential cross sections for transport codes

The light ion differential cross section models developed in the present work are intended for use in the 3-dimensional, deterministic transport code called 3DHZETRN [7, 8, 9, 10, 11]. Consequently, special effort was made to develop highly efficient model parameterizations capable of fast execution times on computers. Transport codes are evaluated in the lab frame and do not require Lorentz-invariant[9] differential cross sections. Instead, the non-invariant double-differential cross section $\frac{d^2\sigma}{dEd\Omega}$ and non-invariant

---

[9]The models were developed in terms of Lorentz-invariant cross sections because Lorentz-invariance makes the mathematical transformations between different reference frames much simpler.

single-differential spectral $\frac{d\sigma}{dE}$ and angular $\frac{d\sigma}{d\Omega}$ cross sections are required. Expressions for $\frac{d^2\sigma}{dEd\Omega}$ and $\frac{d\sigma}{dE}$ will be derived below, while $\frac{d\sigma}{d\Omega}$ will be left for future work.

3.1 Non-invariant double-differential cross section

The non-invariant double-differential cross section $\frac{d^2\sigma}{dEd\Omega}$ is related to the Lorentz-invariant differential cross section [12] for the outgoing pion, π, via[10]

$$\frac{d^2\sigma}{dEd\Omega} = \frac{d^2\sigma}{dTd\Omega} = |\mathbf{p}|\frac{d^3\sigma}{dp^3/E} = \sqrt{T_{\pi L}(T_{\pi L} + 2m_\pi)}\;\frac{d^3\sigma}{dp^3/E}\;, \tag{26}$$

with $dp^3 = p^2 dp d\Omega$, and $p \equiv |\mathbf{p}|$. Also, using $E_{\pi L} \equiv T_{\pi L} + m_\pi = \sqrt{p_{\pi L}^2 + m_\pi^2}$, the substitution $|\mathbf{p}| \equiv p_{\pi L} = \sqrt{T_{\pi L}(T_{\pi L} + 2m_\pi)}$ has been made in order to write cross sections as functions of the pion kinetic energy $T_{\pi L}$ used in transport codes.

3.1.1 Double-differential cross section

Writing equation (2) in terms of kinetic energy and substituting into equation (26) gives the final form of the pion double-differential cross section to be used in transport codes,

$$\frac{d^2\sigma}{dT_{\pi L}d\Omega_{\pi L}} = \mathcal{N}'\sqrt{T_{\pi L}(T_{\pi L} + 2m_\pi)}$$
$$\times \exp\left\{[m_\pi - \gamma_{CL}(T_{\pi L} + m_\pi) + \gamma_{CL}\,\beta_{CL}\,\sqrt{T_{\pi L}(T_{\pi L} + 2m_\pi)}\cos\theta_{\pi L}]/\Theta_\pi\right\}, \tag{27}$$

with the relativistic γ and β factors given in equation (3). The FULL ($F(\theta)$ from Table 1) or SIMPLE ($F(\theta) \equiv 1$) versions are obtained depending on the values of $F(\theta)$.

3.2 Non-invariant single-differential spectral cross section

A spectral distribution for pion production is obtained by integrating $\frac{d^2\sigma}{dEd\Omega}$, as in

$$\frac{d\sigma}{dE} = \frac{d\sigma}{dT} = \int d\Omega \frac{d^2\sigma}{dEd\Omega} = 2\pi \int_{-1}^{1} d\cos\theta \frac{d^2\sigma}{dEd\Omega} = 2\pi \int_{-1}^{1} dz \frac{d^2\sigma}{dEd\Omega}$$
$$= 2\pi|\mathbf{p}| \int_{-1}^{1} d\cos\theta \frac{d^3\sigma}{dp^3/E} = 2\pi|\mathbf{p}| \int_{-1}^{1} dz \frac{d^3\sigma}{dp^3/E}\;,$$

with $z \equiv \cos\theta_{\pi L}$, and assuming azimuthal symmetry. The result is therefore,

$$\boxed{\frac{d\sigma}{dE} = \pi\sqrt{T_{\pi L}(T_{\pi L} + 2m_\pi)} \int_{-1}^{1} dz \frac{d^3\sigma}{dp^3/E}}\;, \tag{28}$$

---

[10]The solid angle is $d\Omega = \sin\theta d\theta d\phi = -d\cos\theta d\phi = -2\pi d\cos\theta$ when integrated over $d\phi$. Integrating gives $\int d\Omega = \int_0^{2\pi} d\phi \int_0^\pi \sin\theta d\theta = -2\pi \int_1^{-1} d\cos\theta = 2\pi \int_{-1}^{1} d\cos\theta = 2\pi \int_{-1}^{1} dz = 4\pi$, with $z \equiv \cos\theta$.

which is the DDRFG2-FULL final expression for the spectral distribution, $\frac{d\sigma}{dE}$, in terms of the Lorentz-invariant double-differential cross section, $\frac{d^3\sigma}{dp^3/E}$. In general, equation (28) needs to be numerically integrated. The DDRFG2-FULL model substitutes equations (2) and (18) into equation (28), with the integral performed numerically. The end of the theoretical development of the DDRFG2-FULL model has now been reached. Recall that the DDRFG2-FULL model utilizes $F(\theta)$ as given in Table 1, and also includes the break in the negative pion spectrum for low energy proton projectile reactions. Sample results are shown in Table 6.

3.3 Spectral distribution

The rest of this section develops the less accurate DDRFG2-SIMPLE model, where $F(\theta) = 1$. An analytic formula for $\frac{d\sigma}{dE}$ will be obtained by integrating the Lorentz-invariant differential cross section over angle. This analytic procedure only works for $F(\theta) = 1$; otherwise the angle integral needs to be carried out numerically. Therefore, in this section $F(\theta)$ is always set equal to unity, and will not appear in any equations.

In order to obtain the pion spectral distribution, the Lorentz-invariant double-differential cross section of equation (2), must be inserted into the right hand side of equation (28). Isolating only the z terms to be integrated, equations (2) and (27) can be written in the general form as

$$E_\pi \frac{d^3\sigma_\pi}{dp_\pi^3} = \mathcal{N}'V\, e^{zW}, \tag{29}$$

and

$$\frac{d^2\sigma_\pi}{dT_\pi d\Omega_\pi} = \mathcal{N}'\sqrt{T_{\pi L}(T_{\pi L} + 2m_\pi)}\, V\, e^{zW}, \tag{30}$$

where V and W are constants with respect to $z \equiv \cos\theta_{\pi L}$. In terms of kinetic energy,

$$V \equiv \exp\{[m_\pi - \gamma_{\mathcal{C}L}\,(T_{\pi L} + m_\pi)]/\Theta\} = e^X, \tag{31}$$
$$W \equiv [\gamma_{\mathcal{C}L}\,\beta_{\mathcal{C}L}\,\sqrt{T_{\pi L}(T_{\pi L} + 2m_\pi)}\,]/\Theta, \tag{32}$$

where the following definition has been used,

$$X \equiv [m_\pi - \gamma_{\mathcal{C}L}\,(T_{\pi L} + m_\pi)]/\Theta_\pi. \tag{33}$$

Use the result

$$\int_{-1}^{1} dz \exp[Wz] = \frac{2}{W}\sinh W, \tag{34}$$

10

and define

$$\mathcal{A} \equiv \frac{V}{W} \sinh W = \frac{1}{2W}(e^{Z^+} - e^{Z^-}), \tag{35}$$

where

$$Z^{\pm} \equiv X \pm W . \tag{36}$$

The $\frac{V}{W} \sinh W$ term in equation (35) contains multiplication of exponential functions, which can lead to overflow or underflow problems in compilers such as *FORTRAN*. It is better to multiply the exponential functions analytically, as in $\frac{1}{2W}(e^{Z^+} - e^{Z^-})$, prior to numerical evaluation, in order to eliminate overflow or underflow problems.

The final form of the DDFRG2-SIMPLE pion spectral distribution is obtained from equation (28) as

$$\boxed{\frac{d\sigma}{dT_{\pi L}} = 4\pi\mathcal{N}'\sqrt{T_{\pi L}(T_{\pi L} + 2m_\pi)}\,\mathcal{A}}\,, \tag{37}$$

where $dE \equiv dT$. Equation (37) is written entirely in terms of pion kinetic energy, $T_{\pi L}$, using equations (31) and (32). Equation (37) is the final form of the spectral distribution for pion production, and it is a very simple and compact, analytic equation involving no integrals, and is therefore a very efficient parameterization of the pion production spectral distribution. No numerical techniques are required for evaluation. However, note that this DDFRG2-SIMPLE pion spectrum result sets $F(\theta) = 1$, and also does *not* include the break in the negative pion spectrum for low energy proton projectile reactions. Sample plots of the pion spectral distributions are provided in Figures 12 - 15. Sample results are in Tables 7 and 8.

3.3.1 Forward-backward spectral distributions

When implementing spectral distributions in 3DHZETRN [7, 8, 9, 10, 11], it is sometimes convenient to separate out particles scattered in the forward versus backward direction, with the forward $(+)$ direction defined as $\theta < 90°$, and backward $(-)$ direction defined as $\theta > 90°$. Equation (28) becomes

$$\frac{d\sigma}{dE} = \frac{d\sigma}{dT} = \left(\frac{d\sigma}{dT}\right)_- + \left(\frac{d\sigma}{dT}\right)_+ \tag{38}$$

$$= 2\pi\sqrt{T_{\pi L}(T_{\pi L} + 2m_\pi)}\left(\int_{-1}^0 dz\frac{d^3\sigma}{dp^3/E} + \int_0^1 dz\frac{d^3\sigma}{dp^3/E}\right), \tag{39}$$

where

$$\left(\frac{d\sigma}{dT}\right)_\pm \equiv \pm 2\pi\sqrt{T_{\pi L}(T_{\pi L} + 2m_\pi)}\int_0^{\pm 1} dz\frac{d^3\sigma}{dp^3/E} . \tag{40}$$

11

Substituting equation (29) into equation (40) gives

$$\left(\frac{d\sigma}{dT}\right)_\pm = \pm 2\pi \mathcal{N}'V \sqrt{T_{\pi L}(T_{\pi L} + 2m_\pi)} \frac{(e^{\pm W} - 1)}{W} .$$ (41)

Define

$$\mathcal{B}_\pm \equiv \frac{1}{2W}(e^{Z^\pm} - e^X) ,$$ (42)

in analogy to equation (35), where

$$\mathcal{A} = \mathcal{B}_+ - \mathcal{B}_- .$$ (43)

Writing similarly to equation (37), gives the final closed-form, analytic expressions for the DDFRG2-SIMPLE forward-backward spectral distributions as

$$\boxed{\left(\frac{d\sigma}{dT}\right)_\pm = \pm 4\pi \mathcal{N}' \sqrt{T_{\pi L}(T_{\pi L} + 2m_\pi)}\ \mathcal{B}_\pm} .$$ (44)

3.4 Units

Unit analysis is very important when implementing the formulas of the present work into transport codes. Therefore, a detailed discussion is now given. The symbol $\sim$ will be used to denote units. Also, angles in steradian (sr) are not written explicitly, because they are not units in the normal sense. The system of units in the present work uses standard particle physics units, with the speed of light $c \equiv 1$. The units of the Lorentz-invariant double-differential cross section are given by[11]

$$E\frac{d^3\sigma}{dp^3} \sim \frac{\mathrm{mb}}{\mathrm{MeV}^2},$$ (45)

where $\sigma \sim \mathrm{mb}$ and $E \sim p \sim \mathrm{MeV}$. Also, note $m \sim \mathrm{MeV}$. Equations (1) and (6) imply that the units of the normalization constant are the same as the Lorentz-invariant double-differential cross section, namely

$$\mathcal{N} \sim \frac{\mathrm{mb}}{\mathrm{MeV}^2},$$ (46)

which is consistent with the explicit formula for $\mathcal{N}$ given in equation (10). Consider now the units of spectral distribution,

$$\frac{d\sigma}{dT} \sim \frac{\mathrm{mb}}{\mathrm{MeV}},$$ (47)

---

[11]Energy units of MeV are used for illustration. GeV can equally be used.

Equations (31) - (32) show that the V and W terms do not carry units, which is denoted

$$V \sim W \sim 1. \tag{48}$$

Therefore, the units of $\frac{d\sigma}{dT}$ in equation (37) are carried by $\mathcal{N}\sqrt{T_{\pi L}(T_{\pi L} + 2m_\pi)}$, as in

$$\frac{d\sigma}{dT} \sim \mathcal{N}\sqrt{T_{\pi L}(T_{\pi L} + 2m_\pi)} \sim \left(\frac{\text{mb}}{\text{MeV}^2}\right)\text{MeV} \sim \frac{\text{mb}}{\text{MeV}} , \tag{49}$$

arriving at the correct units for $\frac{d\sigma}{dT}$.

4 Verification and Validation

4.1 Verification

A variety of verification tests were undertaken to ensure that the computer codes and mathematical formulas in this work were correct. These tests are listed below.

- Computer codes were originally written in *Mathematica*. Independent codes were also written in *FORTRAN* and both codes were verified to give the same results.

- As described previously in the Introduction, there are two different reference frames used to implement the theoretical models, namely the central fireball and target (lab) frames. The thermal model is calculated in the central fireball frame and then Lorentz transformed to the lab frame in which experimental measurements are available and in which transport codes are evaluated. The differential cross sections, $E\frac{d^3\sigma}{dp^3}$, are Lorentz-invariant, but $\frac{d^2\sigma}{dEd\Omega}$ and $\frac{d\sigma}{dE}$ are not Lorentz-invariant. How is one to check that the complicated set of Lorentz transformations to the lab frame have been done correctly? The most powerful test is to fully integrate all differential cross sections over energy and angle to obtain the total cross section σ, which *is* Lorentz-invariant. All the various differential cross sections should give the same answer, σ, when they are integrated. Extensive verification tests were done, giving high confidence that all Lorentz transformations and resulting formulas for differential cross sections, including the analytic formulas described in Section 3.3, are correct.

- Verification checks of the various formulas used for calculating the maximum pion momentum were obtained by taking 2-body limits and making sure that the results were as expected. These are described in the Appendix.

4.2   Validation: Model compared to data

Three models of Lorentz-invariant double-differential cross sections are compared to experimental data in Figures 1 - 11. The most sophisticated model, and the one which will be recommended for use in transport codes, is the DDFRG2-FULL model, shown as the solid red curves, labeled DDFRG. This model is given by equation (2), and uses the normalization of equation (18), with the corrections factors, $F(\theta)$, listed in Table 1. The DDFRG2-SIMPLE model is shown as dashed green curves in Figures 1 - 11, and does not use any correction factors, i.e. $F(\theta) = 1$. The dashed blue curves in Figures 1 - 11 represent the model [13] that is currently used in the HZETRN transport code.

Proton projectile reactions are shown in Figures 1 - 5. The p + ^{12}C → π^- reaction is shown in Figure 1, with pions produced at 0°, and it is seen that the DDFRG2-FULL and DDFRG2-SIMPLE models give the same results and show much better comparison to the data compared to the HZETRN model. Figure 2 shows pions produced at 90°, with both DDFRG2-FULL and HZETRN providing significantly better results compared to DDFRG2-SIMPLE. Figures 3 - 5 show data for much higher proton projectile energies, and again DDFRG2-FULL and HZETRN provide significantly better results compared to DDFRG2-SIMPLE. In general, for proton projectiles, DDFRG2-FULL provides better descriptions of the data compared to HZETRN, which is especially true for the p + ^{12}C → π^- reaction.

Low energy Helium projectile data is shown in Figure 6 at a variety of pion angles, with DDFRG2-FULL and HZETRN providing significantly better results compared to DDFRG2-SIMPLE. Both models, DDFRG2-FULL and HZETRN give the same results for large angles, but DDFRG2-FULL and DDFRG2-SIMPLE give better results at 70°.

Nucleus-nucleus reactions are shown in Figures 7 - 11. The very forward angle at 0° is shown in Figure 7, which is the nucleus-nucleus analog to the proton-nucleus reaction of Figure 1. DDFRG2-FULL is seen to give much better results compared to DDFRG2-SIMPLE and HZETRN. Larger angle data are shown in Figures 8 - 10 for medium mass projectiles, where DDFRG2-FULL and HZETRN are often similar for larger angles, but DDFRG2 is superior to HZETRN for smaller angles, which are more important for space radiation transport. Heavy La projectile data are shown in Figure 11, where all models are of similar good quality.

Overall, it can be seen that the DDFRG2-FULL model provides an improved comparison to data than is obtained with the current HZETRN model [13]. The improved comparison is interesting because the DDFRG2 model consists of a simple analytic formula, as given by equation (2), based on a thermal model applied to all projectile energies. The HZETRN model [13] is more complicated, involving a thermal model at low energy and a parton scaling model at high energy. In addition, the HZETRN model requires a numerical integration to evaluate the cross section normalization constant, whereas it is obtained with a simple analytic formula in DDFRG2 given by equation (18). It can be seen that the DDFRG2-SIMPLE model is far superior than HZETRN for the p + ^{12}C

$\rightarrow \pi^-$ reaction shown in Figure 1, and is of overall comparable quality to HZETRN for the other reactions in Figures 2 - 11. DDFRG2-FULL is always more accurate than the DDFRG2-SIMPLE model.

The HZETRN transport code requires single differential spectral distributions, which are calculated from Lorentz-invariant double-differential cross sections according to equation (28). The integral in equation (28) is currently performed numerically in HZETRN. It was hoped that this numerical integral could be avoided in DDFRG2 (as it was avoided in DDFRG1), with the use of the SIMPLE model analytic formulas developed in Section 3.3. However, as shown in Figures 12 - 15, the DDFRG2-SIMPLE model (with $F(\theta) = 1$) does not compare well with the more accurate DDFRG2-FULL model using $F(\theta) \neq 1$, as given in Table 1. The analytic formulas developed in Section 3.3 will be useful if one is needing only approximate results for the spectral distributions. If one needs highly accurate results, then the numerical integration of equation (28) needs to be performed, but using the DDFRG2-FULL model for the integrand, as given in equations (2) and (18).

5   Summary, conclusions and future work

A new thermal model for pion production in energetic nucleon-nucleus and nucleus-nucleus collisions has been developed in this work. The main advantage of the model is the derivation of a closed-form analytic expression for the Lorentz-invariant double-differential cross section, which needs no numerical integrations or other numerical techniques for evaluation, and is therefore very efficiently evaluated in transport codes. The final form of the model, which is called DDFRG2-FULL, is presented in equations (2) and (18). DDFRG2-FULL has a total of 4 adjustable parameters (Tables 1 and 2), and DDFRG2-FULL has been extensively compared to over 1,000 experimental data points, providing excellent comparisons, including comparisons to data for the p + ^{12}C $\rightarrow \pi^-$ reaction, which show a sharp break in the pion spectrum.

A simpler version, called DDFRG2-SIMPLE, only contains one adjustable parameter (Table 2). It also predicts the p + ^{12}C $\rightarrow \pi^-$ much better than the current pion model used in HZETRN. DDFRG2-SIMPLE is less accurate for the other reactions, but still, DDFRG2-SIMPLE produces results comparable in quality to the current pion model used in HZETRN for these other reactions

Integration of the Lorentz-invariant double-differential cross section results in spectral distributions, which are required for HZETRN and other transport codes. Two versions of the spectral distribution have been developed. The most accurate version in DDFRG2-FULL requires numerical integration of the Lorentz-invariant double-differential cross section, as given by equation (28). A simple, closed-form, analytic formula, requiring no numerical integration, has also been developed in DDFRG2-SIMPLE for the spectral distribution, as given in Section 3.3. This latter version is less accurate but will be useful for approximate calculations.

DDFRG now includes all light particles relevant to the space radiation problem, with the exception of neutrons. DDFRG1 includes production of protons and light ions (deuteron, triton, helion, alpha) and DDFRG2 includes production of pions. Neutrons are the most important remaining light particle not included and are therefore the prime subject for future work, with the development of DDFRG3. Other hadrons, such as kaons, η, and ρ mesons might also need to be included in future work [4].

6 Appendix

6.1 Maximum energy & momentum in central frame

Consider the reaction [17, 18]

$$A + B \to F + X \ , \tag{50}$$

where A and B represent the projectile and target respectively, F is the produced fragment of interest, and X is anything else produced in the reaction. The fact that the other reaction products, X, are left unspecified is what characterizes the reaction as *inclusive*, as opposed to an *exclusive* reaction, where all final states, X, are specified exactly[12]. Inclusive reactions are the reaction types needed for deterministic radiation transport as contained in the code HZETRN [7, 8, 9, 10, 11]. The 3-momentum of particle F in the center-of-momentum frame (denoted with a star $*$) is given by [17, 18]

$$\mathbf{p}_F^{*\,2} = \frac{[s - (m_F + m_X)^2][s - (m_F - m_X)^2]}{4s} \ , \tag{51}$$

where m_F is the mass of the final fragment particle of interest, m_X is the sum of the masses of all the other particles, and s is the Mandelstam variable[13], which can be written in terms of the projectile kinetic energy, $T_{\mathcal{P}L}$, as measured in the lab frame, as

$$s = 2m_B T_{\mathcal{P}L} + (m_A + m_B)^2 \ , \tag{52}$$

where m_A and m_B are the mass of the projectile and target. In the case where A and B are nucleons (N), then

$$s = 2m_N(T_{\mathcal{P}L} + 2m_N) \ , \qquad (NN \to \text{anything}) \ . \tag{53}$$

where m_N is the nucleon mass.

The upper integration limit, $T_{\max}$, for the kinetic energy of particle C in equation (11) can be obtained from equation (51). In order to do so, one must consider the

---

[12]The inclusive cross section is simply the sum of all the exclusive cross section channels.

[13]In the center-of-momentum frame, $\sqrt{s}$ is defined as the total center-of-momentum energy, $\sqrt{s} \equiv E_A + E_B = E_F + E_X$,

exclusive contributions to reaction (50), which can be evaluated from conservation laws [18]. Pion production is the focus of the present work, and conservation laws, particularly conservation of baryon number, determine that the first available (i.e. lowest energy thershold) exclusive channel for nucleon (N) interactions is

$$N + N \rightarrow \pi + N + N, \tag{54}$$

where a nucleon represents either a proton or neutron and π represents any of the three pion charge states (π^+, π^-, π^0). Conservation of baryon number requires two baryons (nucleons, in this case) in the final state if two baryons are present in the initial state. In this case, $m_C = m_\pi$ and $m_X = 2m_N$, and substituting into equation (51) yields the maximum pion momentum (squared) in the center-of-momentum frame,

$$
\begin{aligned}
\mathbf{p}_{\pi\,\text{max}}^{*\,2} &= \frac{[s - (m_\pi + 2m_N)^2][s - (m_\pi - 2m_N)^2]}{4s}, & (NN \rightarrow \pi NN) \quad (55) \\
&= \frac{(2m_N T_{\mathcal{P}L} - 4m_N m_\pi - m_\pi^2)(2m_N T_{\mathcal{P}L} + 4m_N m_\pi - m_\pi^2)}{8m_N(2m_N + T_{\mathcal{P}L})}, & (NN \rightarrow \pi NN) \quad (56)
\end{aligned}
$$

where equation (53) has been substituted for s in equation (55) to give the final equation (56). Using the Einstein equations (4) and (5), gives

$$E_{\pi\,\text{max}}^* = \frac{1}{2\sqrt{2}}\sqrt{\frac{(2m_N T_{\mathcal{P}L} + m_\pi^2)^2}{m_N(2m_N + T_{\mathcal{P}L})}}, \qquad (NN \rightarrow \pi NN), \tag{57}$$

or

$$T_{\pi\,\text{max}}^* = \frac{1}{2\sqrt{2}}\sqrt{\frac{(2m_N T_{\mathcal{P}L} + m_\pi^2)^2}{m_N(2m_N + T_{\mathcal{P}L})}} - m_\pi, \qquad (NN \rightarrow \pi NN), \tag{58}$$

to be substituted as the upper kinetic energy integration limit in equation (11).

For comparison with DDFRG1 [5, 6] for proton production in nucleon-nucleon collisions, consider the reaction

$$N + N \rightarrow N + N. \tag{59}$$

With $m_F = m_N$ and $m_X = m_N$, equation (51) gives the maximum nucleon momentum in the center of momentum frame,

$$\mathbf{p}_{N\,\text{max}}^{*\,2} = \frac{s}{4} - m_N^2 = \frac{1}{2}m_N T_{\mathcal{P}L}, \qquad (NN \rightarrow NN), \tag{60}$$

where equation (53) is substituted for s to give the final formula. Using the Einstein equations (4) and (5), gives

$$E_{N\,\text{max}}^* = \sqrt{m_N\left(m_N + \frac{T_{\mathcal{P}L}}{2}\right)}, \qquad (NN \rightarrow NN), \tag{61}$$

or

$$T^*_{N\,\text{max}} = \sqrt{m_N(m_N + \frac{T_{\mathcal{P}L}}{2})} - m_N \ , \qquad (NN \to NN), \qquad (62)$$

to be substituted as the upper kinetic energy integration limit in equation (11).

6.2 Maximum energy & momentum in lab frame

The nucleon-nucleon center of momentum $(NNCM)$ frame has been denoted with the $*$ symbol. The central fireball frame is denoted with the $\mathcal{C}$ symbol. For particles produced from nucleon-nucleon collisions, these two frames are the same $(* = \mathcal{C})$, so that either symbol can be used. It will be more convenient below to use the $\mathcal{C}$ symbol. The Lorentz transformation of the pion energy from the central $(\mathcal{C} = NNCM)$ frame to the lab (L) frame [12] is given by

$$E_{\pi L} \;=\; \gamma_{\mathcal{C}L}\left(E_{\pi\mathcal{C}} + \beta_{\mathcal{C}L}\sqrt{E^2_{\pi\mathcal{C}} - m^2_\pi}\cos\theta_{\pi\mathcal{C}}\right) \ , \qquad (63)$$

where $E_{\pi L}$ is the pion total energy in the lab frame, $E_{\pi\mathcal{C}}$ and $\theta_{\pi\mathcal{C}}$ are the pion total energy and angle in the central frame, and m_π is the pion mass. The relativistic γ factor relating the velocity of the central (NNCM) frame relative to the lab frame is given by [12]

$$\gamma_{\mathcal{C}L} = \frac{E_{\text{lab}} + m_B}{\sqrt{s}} = \frac{T_{\mathcal{P}L} + m_A + m_B}{\sqrt{s}} = \frac{T_{\mathcal{P}L} + 2m_N}{\sqrt{s}} \ , \qquad (64)$$

where $E_{\text{lab}} = T_{\mathcal{P}L} + m_B$ is the total energy of the projectile (A), as measured in the lab frame. For nucleon-nucleon collisions, $m_A = m_B \equiv m_N$, resulting in simplification on the far right hand side. The Mandelstam variable [12] is

$$\sqrt{s} = \sqrt{m^2_A + m^2_B + 2m_B E_{\text{lab}}} = \sqrt{2m_N(T_{\mathcal{P}L} + 2m_N)} \ , \qquad (65)$$

with simplification on the far right hand side again arising for nucleon-nucleon collisions. The relativistic speed is

$$\beta_{\mathcal{C}L} = \sqrt{1 - \frac{1}{\gamma^2_{\mathcal{C}L}}} \ , \qquad (66)$$

In equation (63), the *maximum* pion total energy in the lab frame is obtained by setting $\cos\theta_{\pi\mathcal{C}} = 1$, and by substituting the maximum pion energy from equation (57) into equation (63), $E_{\pi\mathcal{C}} = E^*_{\pi\,\text{max}}$, giving

$$
\begin{aligned}
E_{\pi L\,\text{max}} \;\equiv\; T_{\pi L\,\text{max}} + m_\pi &= \sqrt{\mathbf{p}^2_{\pi L\,\text{max}} + m^2_\pi} \qquad\qquad\qquad (NN \to \pi NN)\\[2mm]
&= \frac{1}{4m_N}\left[2m_N T_{\mathcal{P}L} + m^2_\pi + \sqrt{\frac{T_{\mathcal{P}L}[m^4_\pi - 4m^2_\pi m_N T_{\mathcal{P}L} + 4m^2_N(T^2_{\mathcal{P}L} - 4m^2_\pi)]}{T_{\mathcal{P}L} + 2m_N}}\right] ,
\end{aligned}
$$

$$(67)$$

18

from which the magnitude of the maximum pion momentum in the lab (= target) frame, $p_{\pi L \text{ max}} \equiv |\mathbf{p}_{\pi L \text{ max}}| = \sqrt{\mathbf{p}_{\pi L \text{ max}}^2}$, is easily extracted.

Again, for comparison with DDFRG1, evaluate the above result for $NN \to NN$, and again in equation (63), the maximum nucleon total energy in the lab frame is obtained by setting $\cos \theta_{\pi \mathcal{C}} = 1$, and by substituting the maximum nucleon energy from equation (61) into equation (63), where in equation (63) π symbols are replaced by N, giving

$$
\begin{aligned}
E_{NL \text{ max}} &\equiv T_{NL \text{ max}} + m_N = \sqrt{\mathbf{p}_{NL \text{ max}}^2 + m_N^2} \\
&= T_{\mathcal{P}L} + m_N \qquad\qquad\qquad\qquad (NN \to NN). \qquad (68)
\end{aligned}
$$

The complicated set of manipulations, including derivation of the maximum nucleon momentum in the central frame, and subsequent Lorentz transformation to the lab frame have resulted in the very simple result shown in equation (68). This provides a very nice verification check on all the preceeding formulas, because it is exactly the result one would expect for the two body $NN \to NN$ reaction, where the maximum kinetic energy of the outgoing nucleon is simply the projectile nucleon kinetic energy, $T_{NL \text{ max}} = T_{\mathcal{P}L}$.

7 Tables

Table 1: Correction factors, $F(\theta)$, for pion cross sections. The symbol, $T_{\mathcal{P}L}$, is the kinetic energy of the projectile relative to the lab, $\theta_{\pi L}$ is the angle of the emitted pion in the lab (target) frame, and Z is the charge of the projectile. The interpretation of the table is as follows: For projectile kinetic energies ≤ 10 GeV/n and pion lab angles $< 30°$, multiply the pion cross sections by 3, for projectiles Li to Zn ($3 \leq Z \leq 30$). For projectile kinetic energies ≤ 10 GeV/n and pion lab angles $\geq 90°$, multiply the cross sections by 1.5, for all projectiles. For projectile kinetic energies > 10 GeV/n, multiply the cross sections by 0.57, for all pion angles and all projectiles. If the above conditions do not hold, then no correction is applied, i.e. $F(\theta) \equiv 1$.

$T_{\mathcal{P}L}$ (GeV/n)	$\theta_{\pi L}$	$F(\theta)$	Z
≤ 10	$< 30°$	3	$3 \leq Z \leq 30$
≤ 10	$\geq 90°$	1.5	all
> 10	all	0.57	all

Table 2: Thermal spectrum parameters after momentum break points. The temperature of the central fireball pion source after momentum break, $\Theta_{\pi\,break}$, is 0.2 multiplied by the central fireball pion temperature. The modified thermal spectrum is only implemented for negative pion production from proton-nucleus reactions with pion emission lab angles smaller than a critical angle of 5°, and pion lab momenta greater than p_{break}.

Break temperature	$\Theta_{\pi\,\text{break}} = 0.2 \times \Theta_\pi$
Critical angle	5°

Table 3: Calculated break points, p_{break}, for the reaction p + ^{12}C $\rightarrow \pi^-$. The kinetic energy of the proton projectile is labelled, T_{p}, in units of GeV. The calculated break points are seen to occur exactly where the experimental data shown in Figure 1 display a transition, or break, to a different temperature.

T_{p} (GeV)	1.05	2.1
p_{break} (GeV)	0.82	1.80

Table 4: Sample results for DDFRG Full Parameter model Lorentz-invariant differential cross sections in lab frame. The symbol, $T_{\mathcal{P}L}$, is the kinetic energy of the projectile relative to the lab frame.

Reaction	$T_{\mathcal{P}L}$ MeV/n	$p_{\pi L}$ MeV	$T_{\pi L}$ MeV	$\theta_{\pi L}$ deg	$E_{\pi L}\frac{d^3\sigma_\pi}{dp_\pi^3}(p_{\pi L},\theta_{\pi L})$ mb MeV^{-2}sr^{-1}		
					π^+	π^-	π^0
p + C	2100	1000	869.752	0	2.665×10^{-5}	1.413×10^{-5}	2.215×10^{-5}
		2200	2064.45	0	2.455×10^{-7}	2.487×10^{-10}	2.040×10^{-7}
p + Be	17,500	1000	869.752	8.8	1.540×10^{-4}	1.948×10^{-4}	1.535×10^{-4}
		4000	3862.45	12.1	3.375×10^{-6}	4.269×10^{-6}	3.364×10^{-6}
He + Al	400	100	32.0465	70	3.1147×10^{-4}	4.085×10^{-4}	2.968×10^{-4}
		150	65.1828	130	3.457×10^{-5}	4.534×10^{-5}	3.294×10^{-5}
La + La	800	200	104.131	20	3.35455×10^{-2}	4.6463×10^{-2}	6.32999×10^{-2}
		600	476.117	80	1.30066×10^{-5}	1.80149×10^{-5}	2.45433×10^{-5}

Table 5: Sample results for DDFRG SIMPLE No-Parameter model Lorentz-invariant differential cross sections in lab frame. The symbol, $T_{\mathcal{P}L}$, is the kinetic energy of the projectile relative to the lab frame.

Reaction	$T_{\mathcal{P}L}$ MeV/n	$p_{\pi L}$ MeV	$T_{\pi L}$ MeV	$\theta_{\pi L}$ deg	$E_{\pi L}\frac{d^3\sigma_\pi}{dp_\pi^3}(p_{\pi L},\theta_{\pi L})$ mb MeV^{-2}sr^{-1}		
					π^+	π^-	π^0
p + C	2100	1000	869.752	0	2.6650×10^{-5}	1.41280×10^{-5}	2.21453×10^{-5}
		2200	2064.45	0	2.4549×10^{-5}	2.48733×10^{-10}	2.03989×10^{-7}
p + Be	17,500	1000	869.752	8.8	2.70212×10^{-4}	3.41777×10^{-4}	2.69328×10^{-4}
		4000	3862.45	12.1	5.92187×10^{-6}	7.49025×10^{-6}	5.90248×10^{-6}
He + Al	400	100	32.0465	70	3.1147×10^{-4}	4.0852×10^{-4}	2.9676×10^{-4}
		150	65.1828	130	2.3045×10^{-5}	3.0226×10^{-5}	2.1967×10^{-5}
La + La	800	200	104.131	20	3.35455×10^{-2}	4.646252×10^{-2}	6.32999×10^{-2}
		600	476.117	80	1.30066×10^{-5}	1.80149×10^{-5}	2.4543×10^{-5}

Table 6: Sample results for DDFRG Full Parameter model spectral distributions in the lab frame. $F(\theta)$ is obtained from Table 1.

Reaction	$T_{\mathcal{P}L}$ MeV/n	$T_{\pi L}$ MeV	$\frac{d\sigma}{dT}$ mb MeV^{-1}		
			π^+	π^-	π^0
p + C	2100	500	0.0648216	0.0343637	0.0538642
He + C	400	100	0.0882712	0.11247	0.0758925
C + C	1050	100	1.35627	1.28578	1.40954
Fe + Al	2100	500	4.88606	5.32836	7.4918

Table 7: Sample results for SIMPLE No-Parameter ($F(\theta)$=1) model spectral distributions in the lab frame.

Reaction	$T_{\mathcal{P}L}$ MeV/n	$T_{\pi L}$ MeV	$\frac{d\sigma}{dT}$ mb MeV^{-1}		
			π^+	π^-	π^0
p + C	2100	500	0.0647774	0.0343403	0.0538275
He + C	400	100	0.0848113	0.108062	0.0729178
C + C	1050	100	0.883573	0.837653	0.918275
Fe + Al	2100	500	2.24748	2.45092	3.44606

Table 8: Sample results for SIMPLE No-Parameter ($F(\theta)$=1) model total cross sections.

| Reaction	$T_{\mathcal{P}L}$ MeV/n	σ mb		
		π^+	π^-	π^0
p + C	2100	92.4088	48.9885	76.7881
He + C	400	19.6442	25.0296	16.8894
C + C	1050	243.51	230.855	253.074
Fe + Al	2100	3206.16	3496.39	4916.01

8 Figures
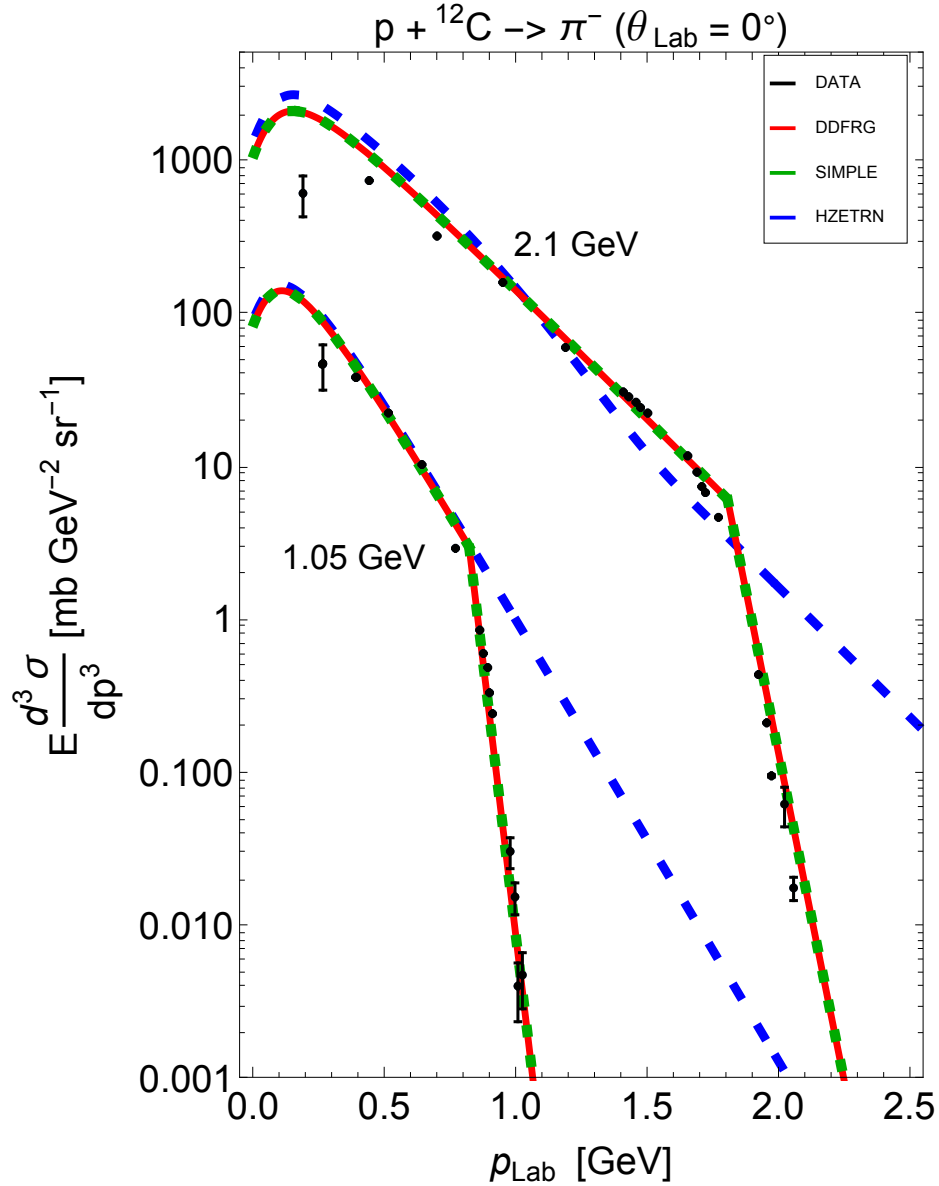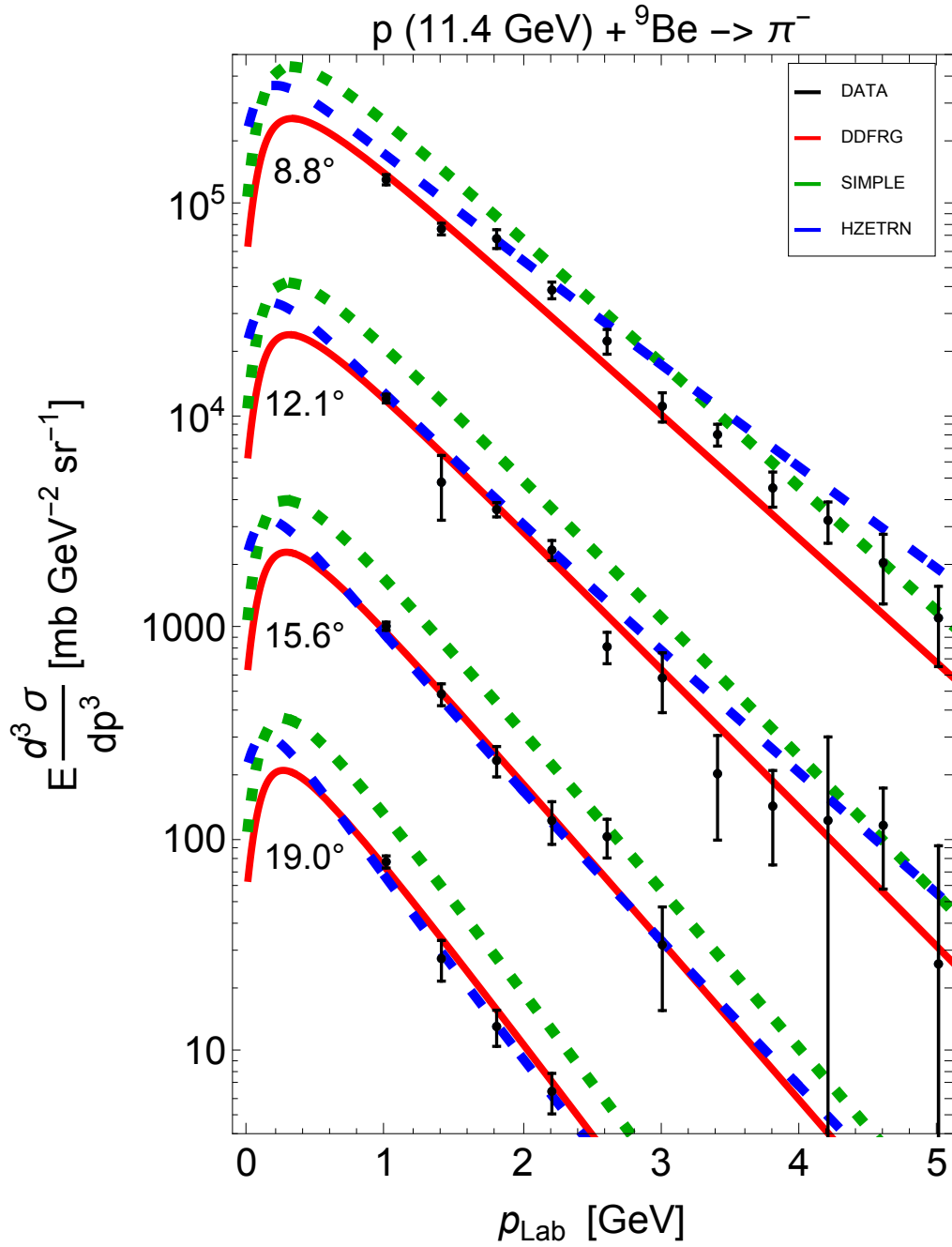

Figure 1: Lorentz-invariant double-differential cross sections as a function of lab frame pion momentum for π^- production at a lab angle of $0°$ from p + ^{12}C reactions. Proton projectile energies are 2.1 GeV and 1.05 GeV. Cross sections for 2.1 GeV have been multiplied by 10 for visual clarity. Data points are shown as black symbols. The pion model [13] currently used in HZETRN is shown as a blue dashed line. The new DDFRG2-FULL model is shown as a red solid line, labeled DDFRG. The DDFRG2-SIMPLE model, which sets the correction factor $F(\theta) \equiv 1$, is shown as a green dashed line.
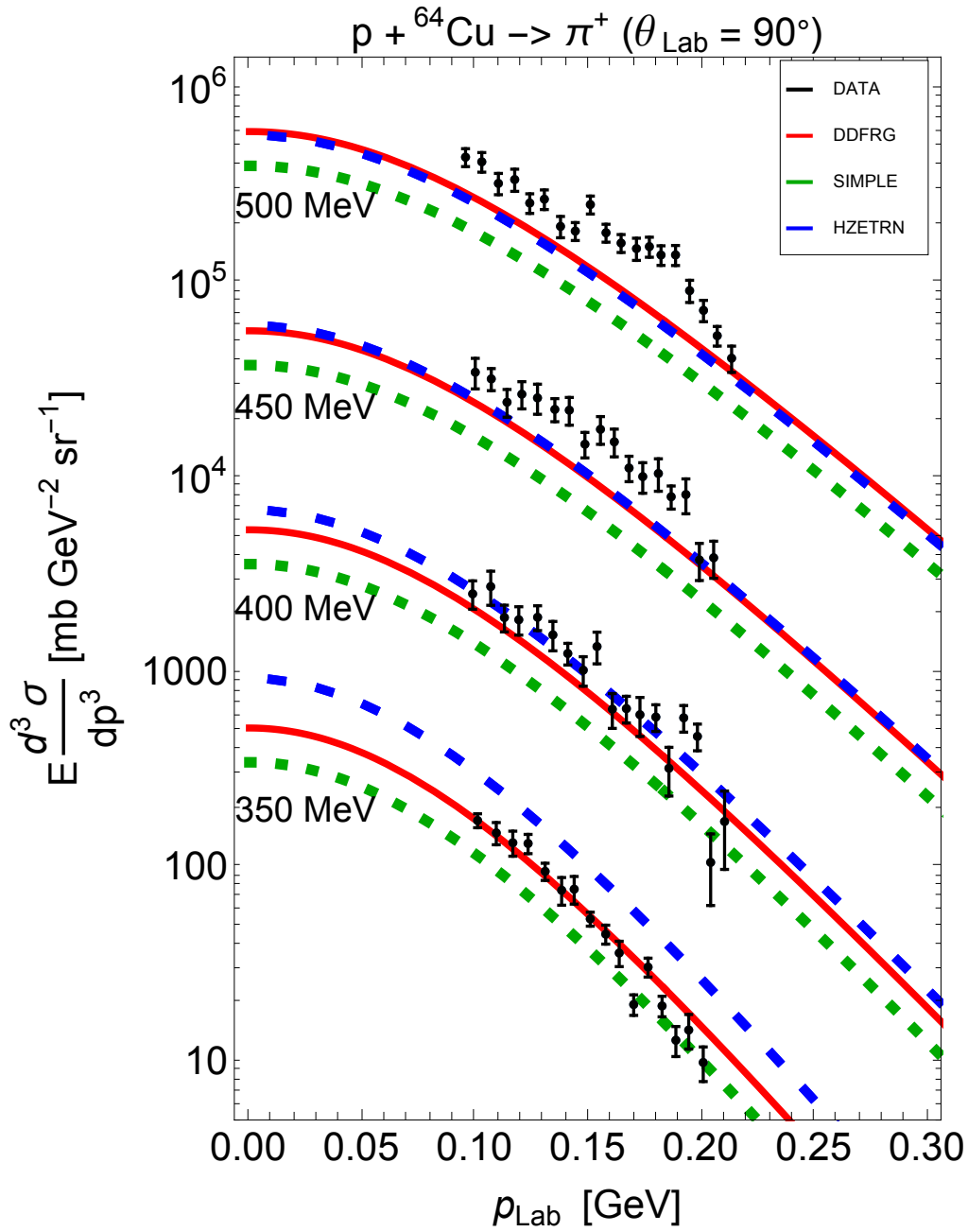
Figure 2: Lorentz-invariant double-differential cross sections as a function of lab frame pion momentum for π^+ production at a lab angle of 90° from p + ^{64}Cu reactions. Proton projectile energies are 500 MeV, 450 MeV, 400MeV, and 350 MeV. Cross sections for 500 MeV, 450 MeV, 400MeV, have been multiplied by 1000, 100, and 10 respectively for visual clarity. Plot color legends are the same as Figure 1.
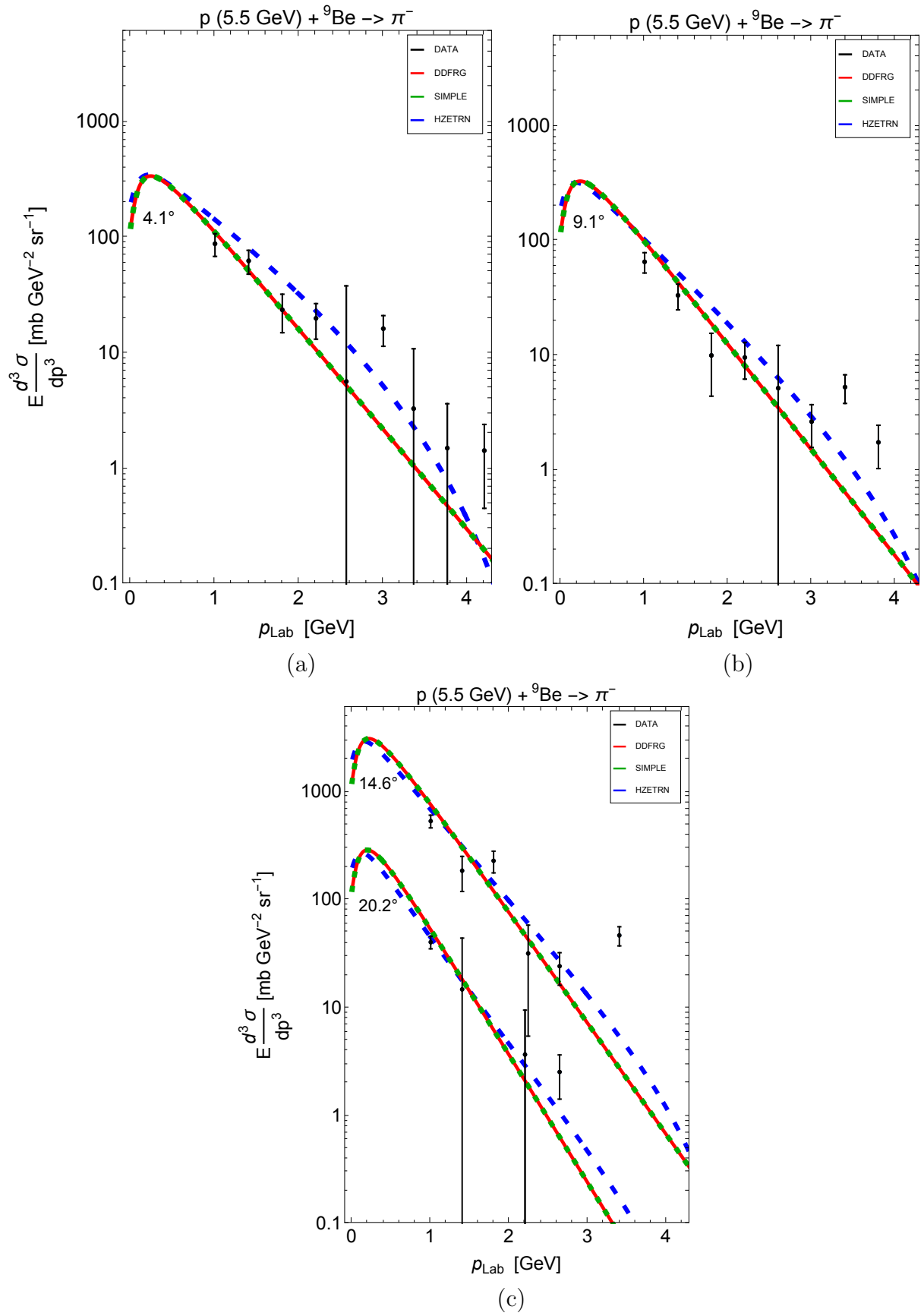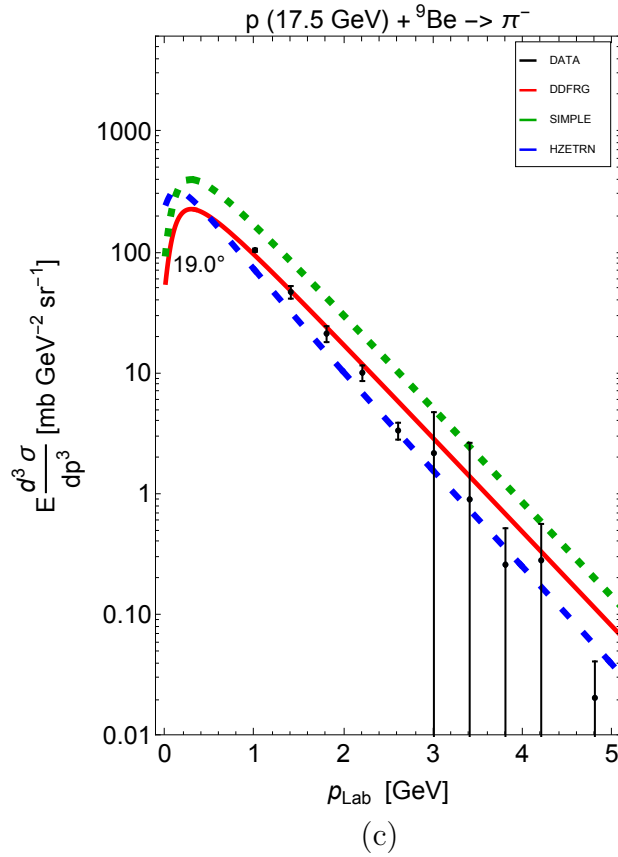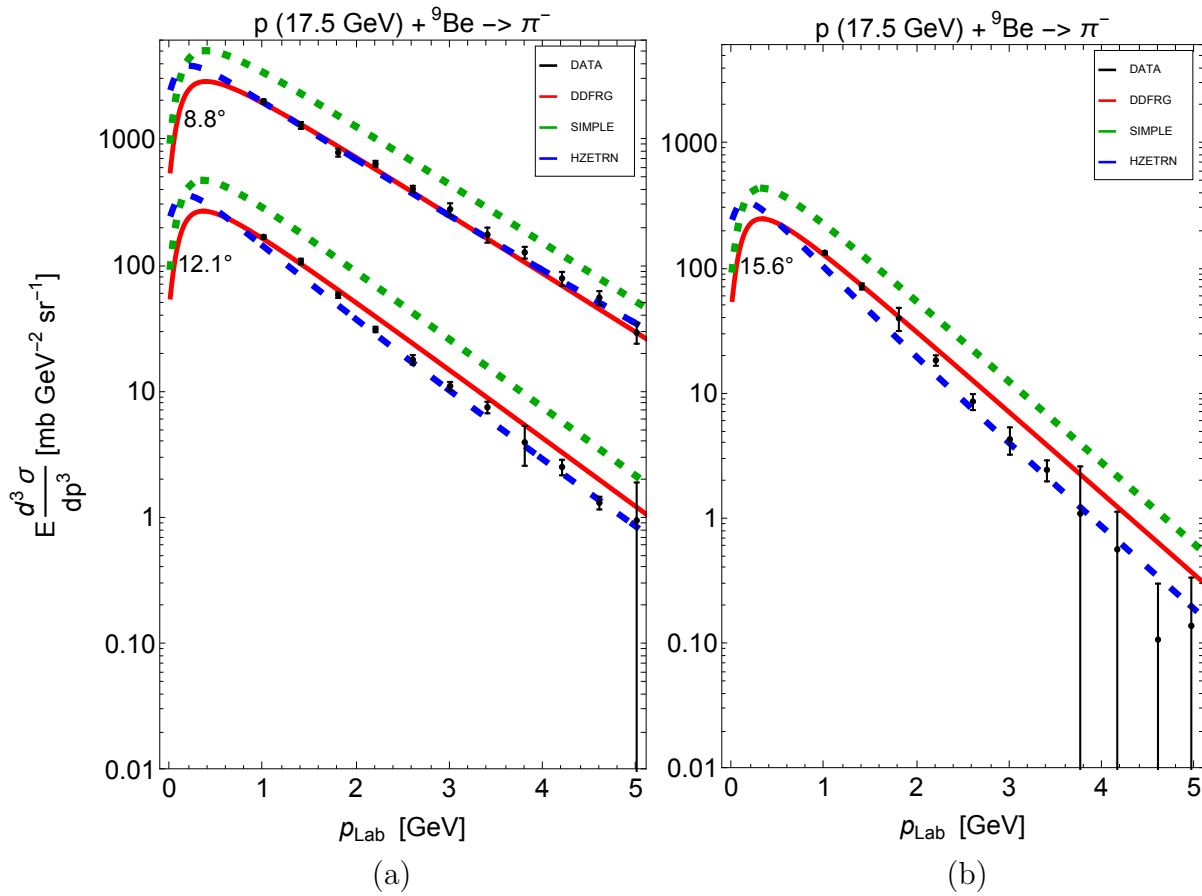
Figure 3: Lorentz-invariant double-differential cross sections as a function of lab frame pion momentum for π^- production from p (5.5 GeV) + ^{9}Be reactions. Lab frame pion production angles are (a) 4.1°, (b) 9.1°, (c) 14.6° and 20.2°. Cross sections for 14.6° have been multiplied by 10 for visual clarity. Plot color legends are the same as Figure 1.
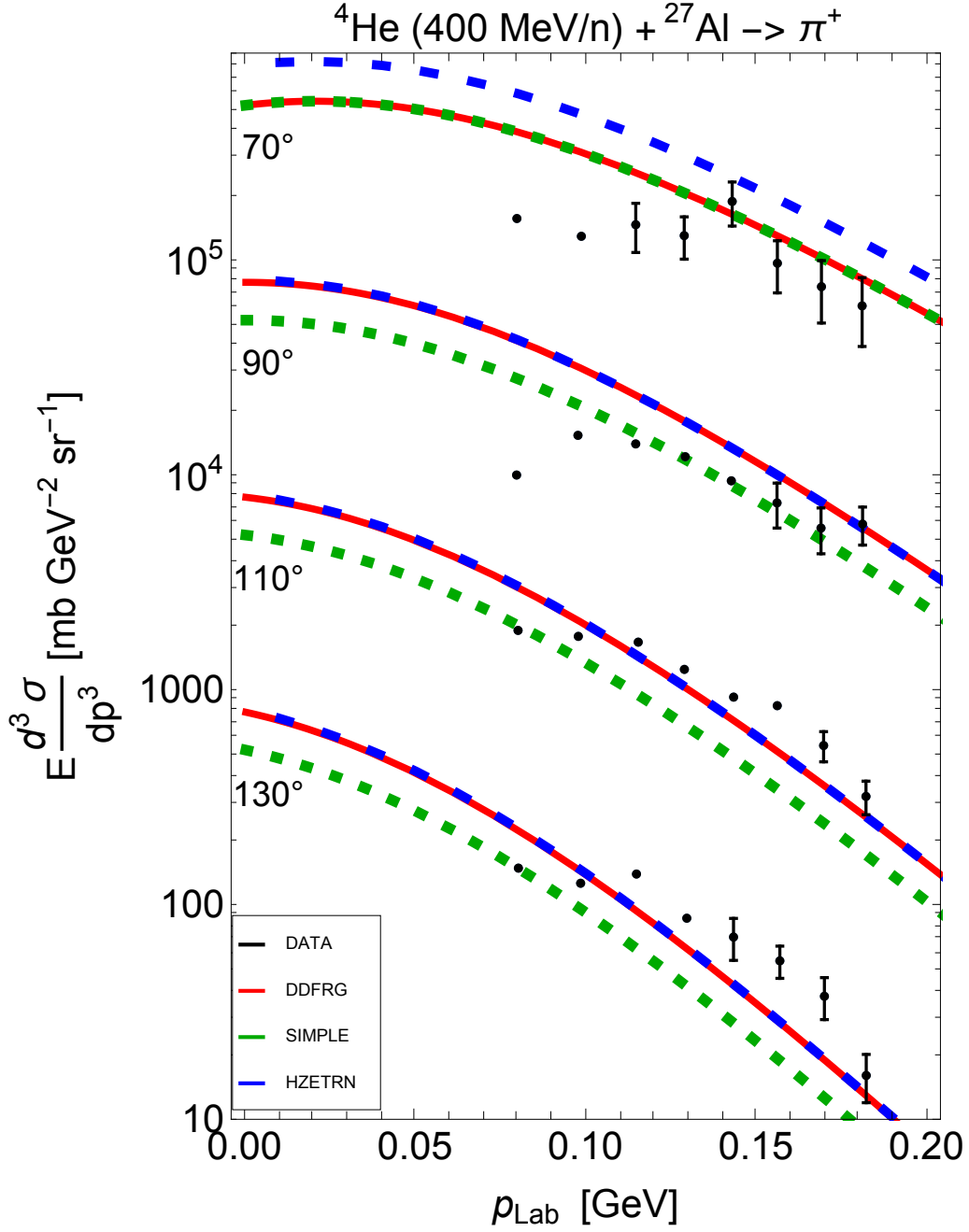
Figure 4: Lorentz-invariant double-differential cross sections as a function of lab frame pion momentum for π^- production from p (11.4 GeV) + ^{9}Be reactions. Lab frame pion production angles are 8.8°, 12.1°, 15.6°, and 19.0°. Cross sections for 8.8°, 12.1°, and 15.6° have been multiplied by 1000, 100, and 10 respectively for visual clarity. Plot color legends are the same as Figure 1.
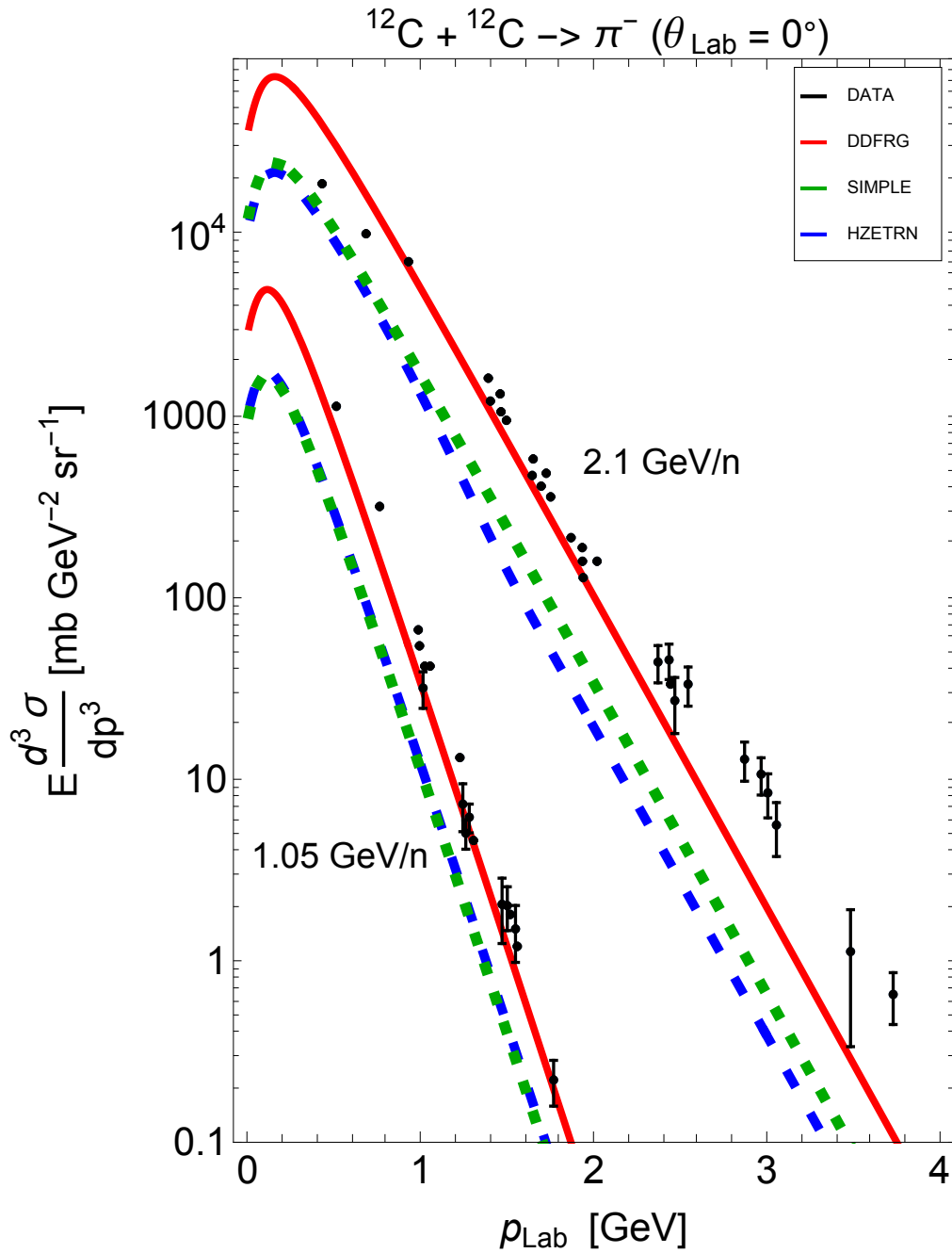
Figure 5: Lorentz-invariant double-differential cross sections as a function of lab frame pion momentum for π^- production from p (17.5 GeV) + ^{9}Be reactions. Lab frame pion production angles are (a) 8.8° and 12.1°, (b) 15.6°, (c) 19.0°. Cross sections for 8.8° have been multiplied by 10 for visual clarity. Plot color legends are the same as Figure 1.

Figure 6: Lorentz-invariant double-differential cross sections as a function of lab frame pion momentum for positive pion (π^+) production from ^{4}He $(400\,\mathrm{MeV/n}) + {}^{27}$Al reactions. Lab frame pion production angles are 70°, 90°, 110°, and 130°. Cross sections for 70°, 90°, and 110°, have been multiplied by 1000, 100, and 10 respectively for visual clarity. Plot color legends are the same as Figure 1.

Figure 7: Lorentz-invariant double-differential cross sections as a function of lab frame pion momentum for π^- production at a lab angle of 0° from ^{12}C + ^{12}C reactions. Projectile energies are 2.1 GeV/n and 1.05 GeV/n. Cross sections for 2.1 GeV/n have been multiplied by 10 for visual clarity. Plot color legends are the same as Figure 1.
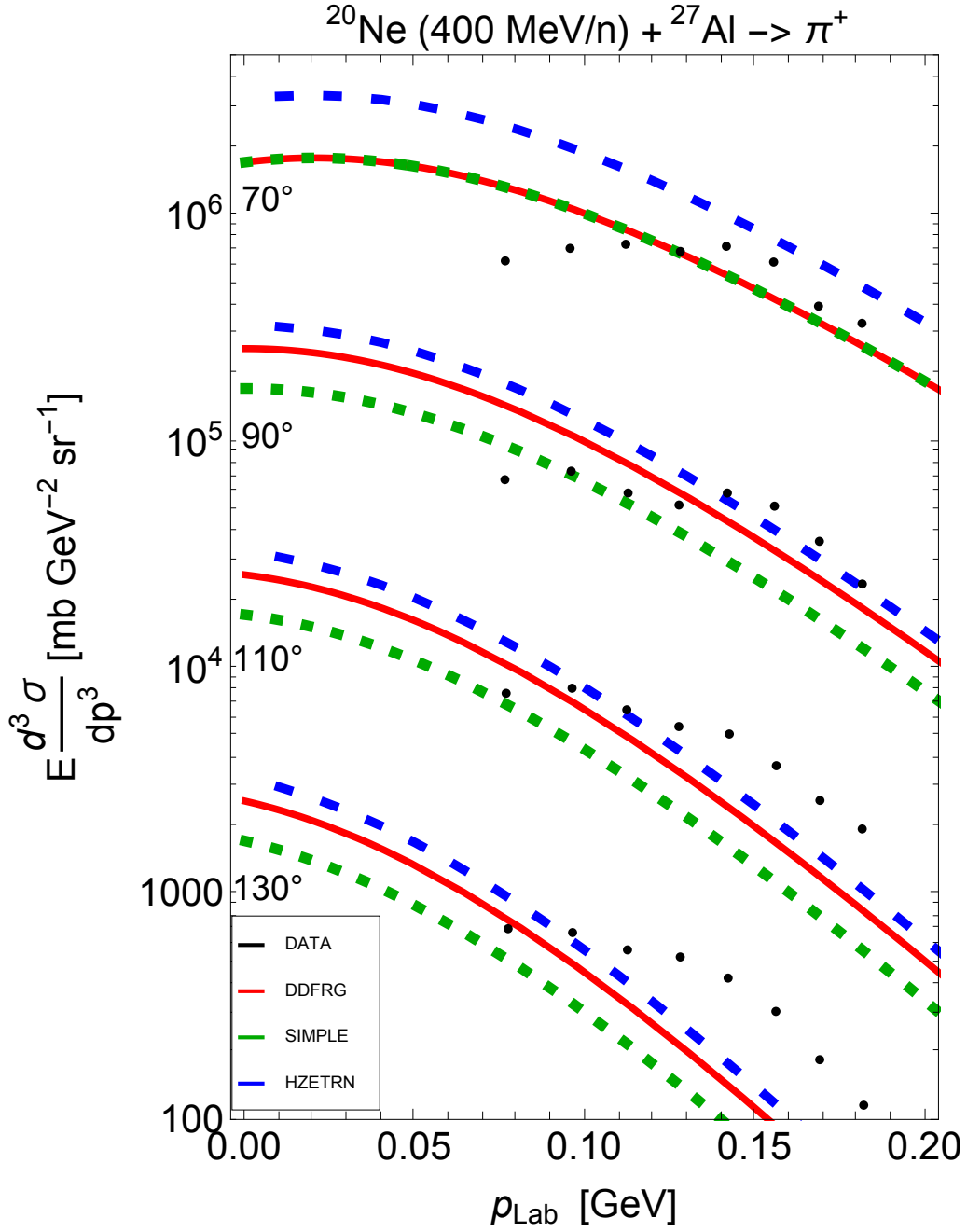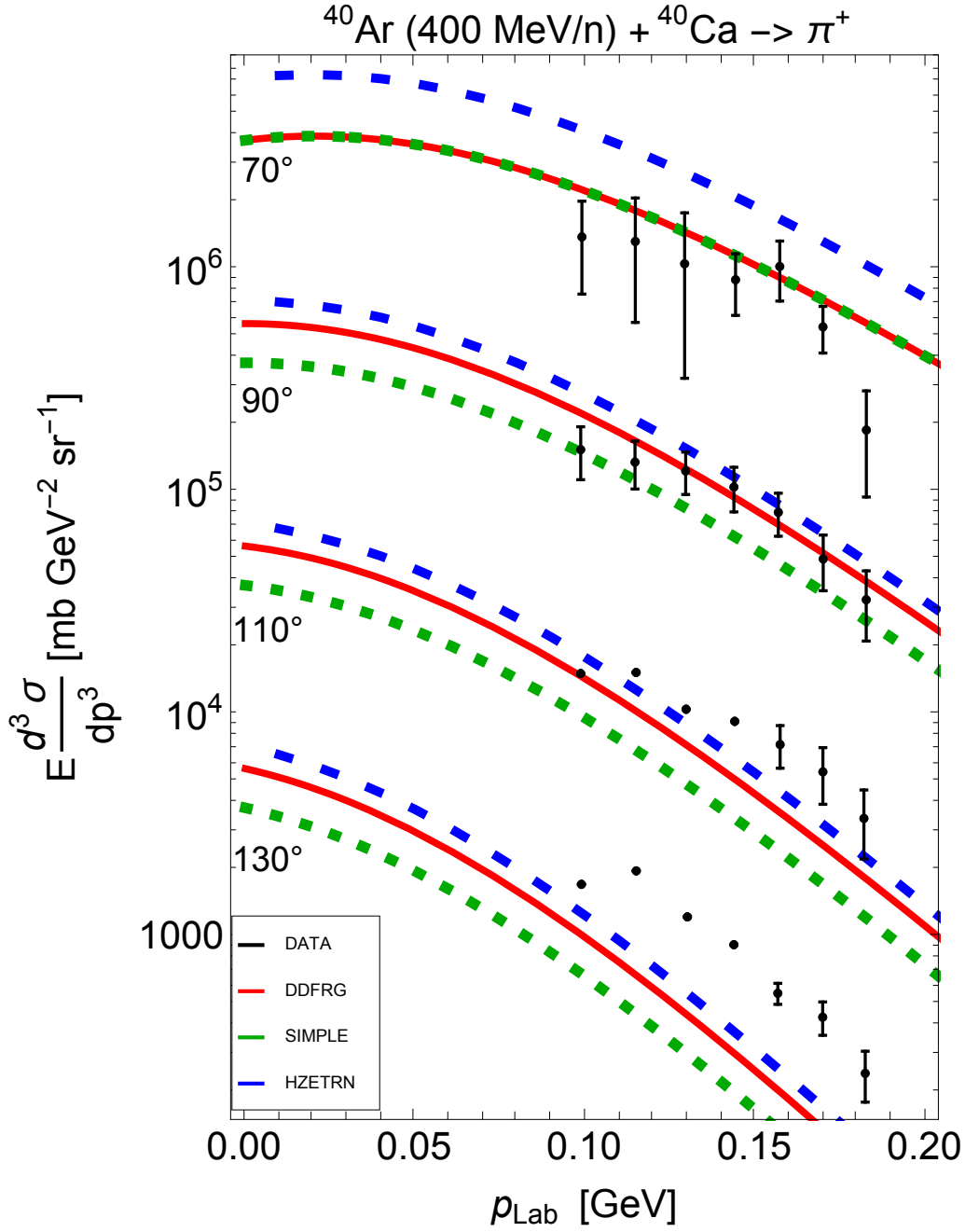
Figure 8: Lorentz-invariant double-differential cross sections as a function of lab frame pion momentum for positive pion (π^+) production from ^{20}Ne (400 MeV/n) + ^{27}Al reactions. Lab frame pion production angles are 70°, 90°, 110°, and 130°. Cross sections for 70°, 90°, and 110°, have been multiplied by 1000, 100, and 10 respectively for visual clarity. Plot color legends are the same as Figure 1.
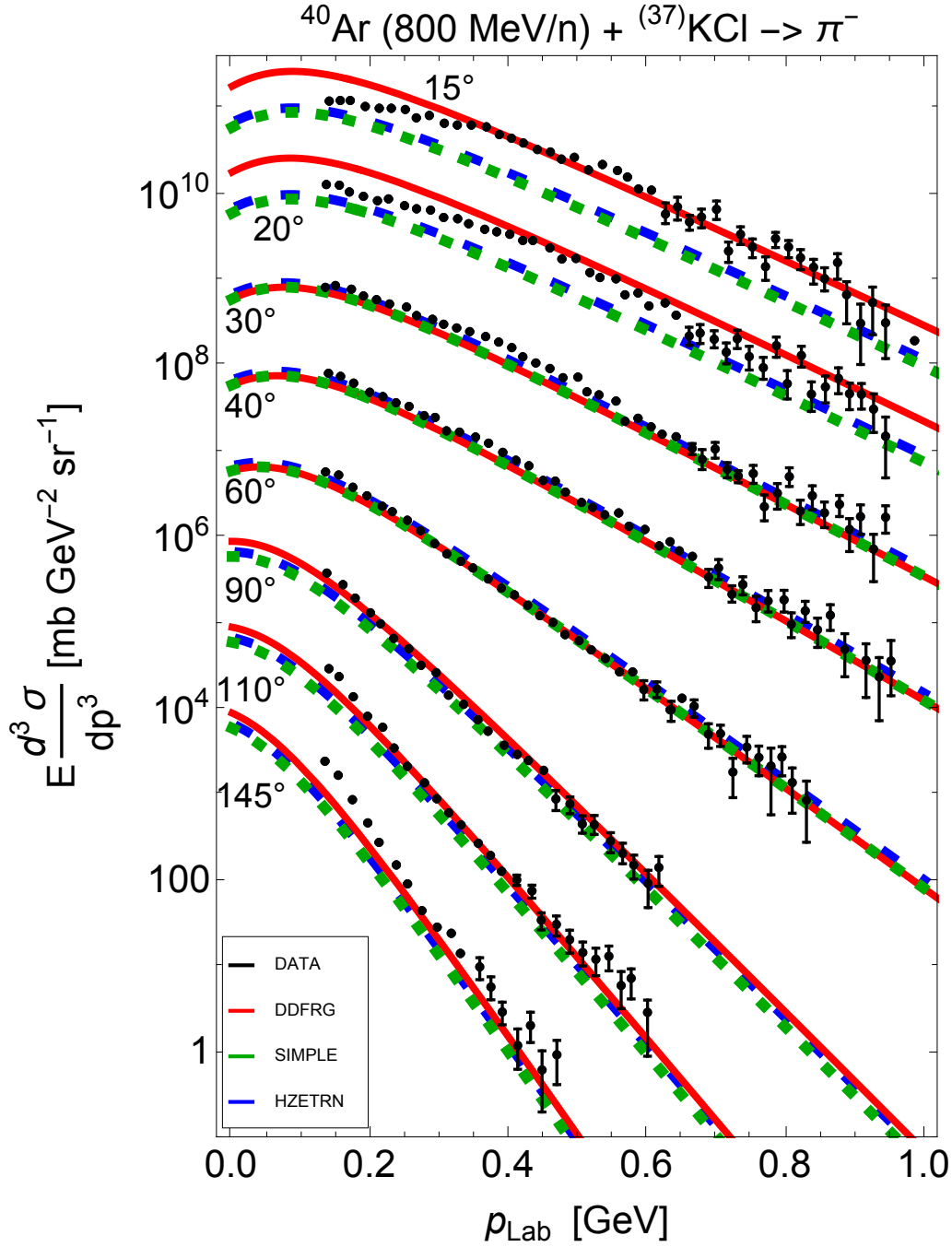
Figure 9: Lorentz-invariant double-differential cross sections as a function of lab frame pion momentum for positive pion (π^+) production from ^{40}Ar (400 MeV/n) + ^{40}Ca reactions. Lab frame pion production angles are 70°, 90°, 110°, and 130°. Cross sections for 70°, 90°, and 110°, have been multiplied by 1000, 100, and 10 respectively for visual clarity. Plot color legends are the same as Figure 1.
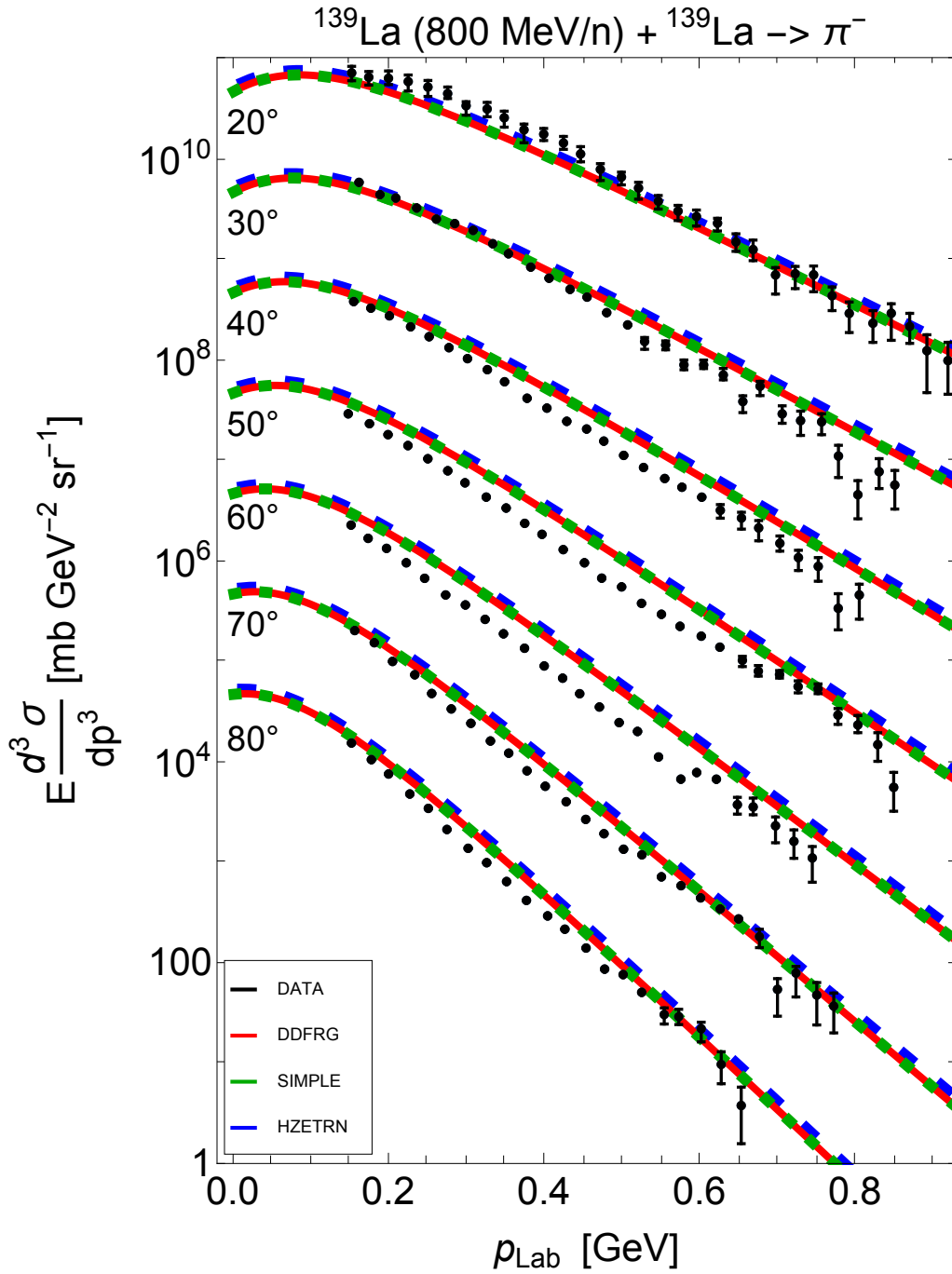
Figure 10: Lorentz-invariant double-differential cross sections as a function of lab frame pion momentum for negative pion π^- production from ^{40}Ar (800 MeV/n) + KCl reactions. Lab frame pion production angles are indicated. Cross sections for 15°, 20°, 30°, 40°, 60°, 90°, and 110° have been multiplied by 10^7, 10^6, 10^5, 10^4, 10^3, 10^2, and 10, respectively for visual clarity. Plot color legends are the same as Figure 1.

Figure 11: Lorentz-invariant double-differential cross sections as a function of lab frame pion momentum for negative pion π^- production from ^{139}La (800 MeV/n) + ^{139}La reactions. Lab frame pion production angles are indicated. Cross sections for 20°, 30°, 40°, 50°, 60°, and 70°, have been multiplied by 10^6, 10^5, 10^4, 10^3, 10^2, and 10, respectively for visual clarity. Plot color legends are the same as Figure 1.
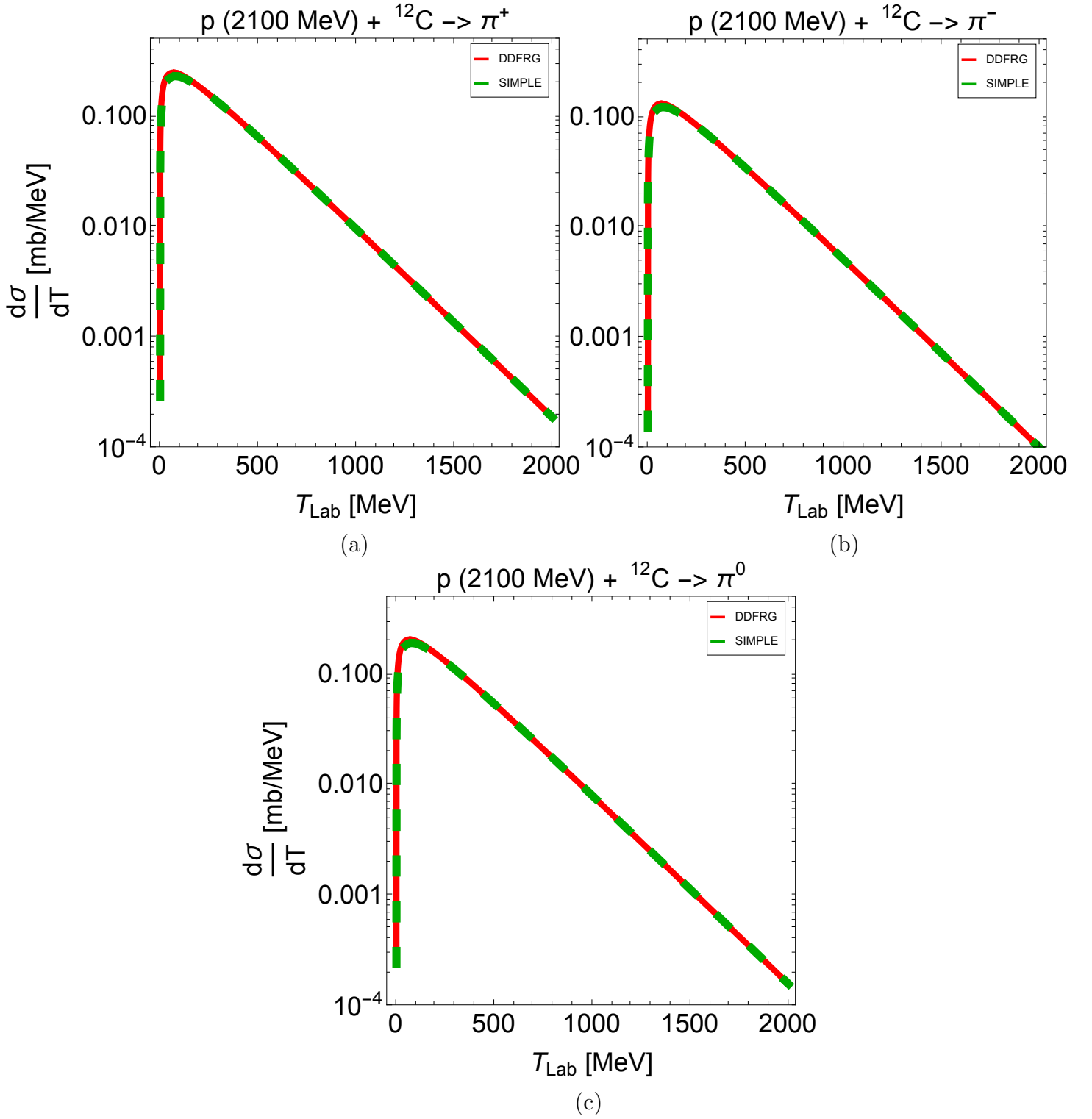
Figure 12: Spectral distribution cross sections as a function of lab frame pion kinetic energy for (a) π^+, (b) π^-, and (c) π^0 production from p (2100 MeV) + ^{12}C reactions. The DDFRG2-FULL model is shown as a red solid line, labeled DDFRG. The DDFRG2-SIMPLE model, with the correction factor $F(\theta) \equiv 1$, is shown as a green dashed line.
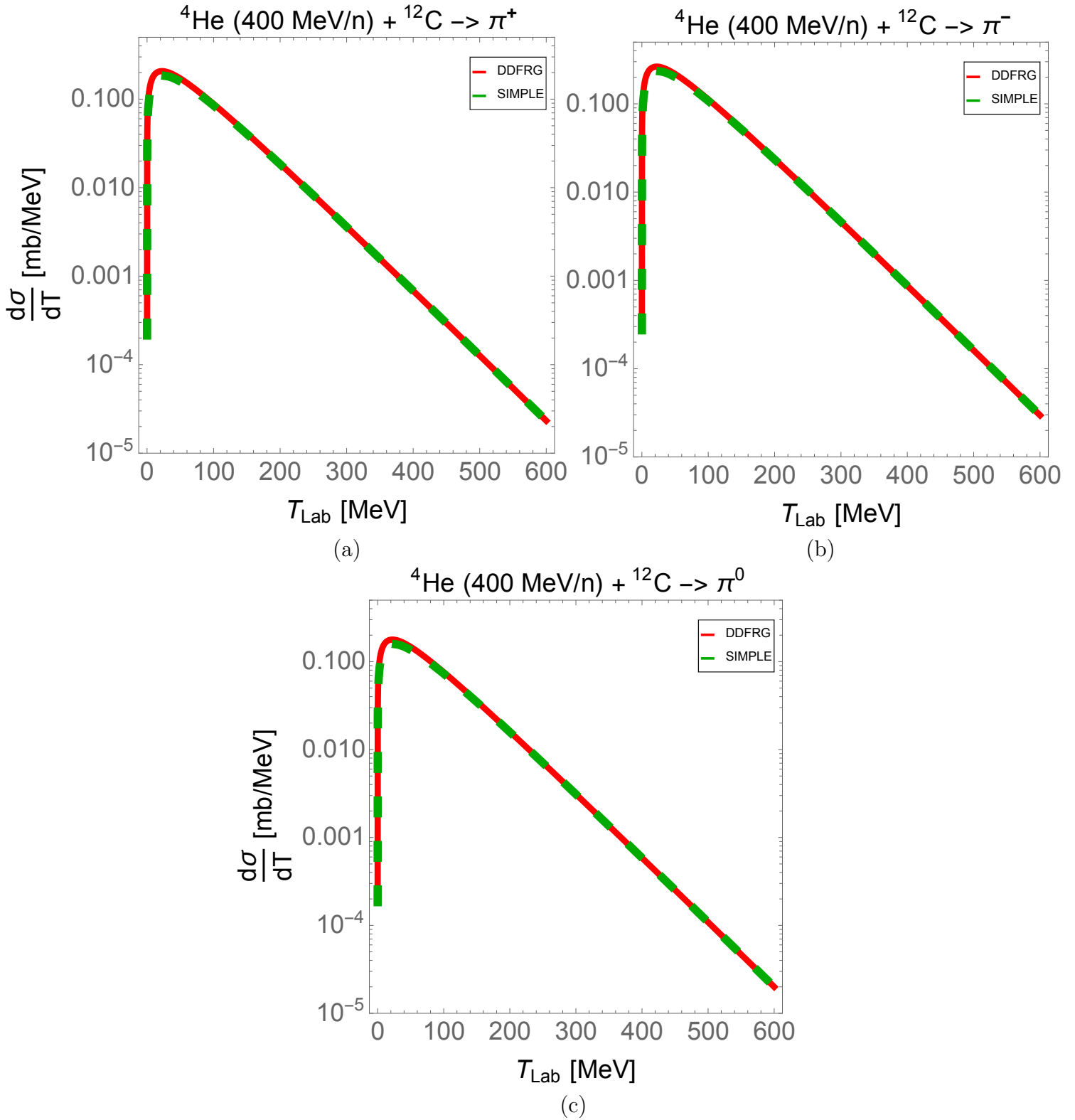
Figure 13: Spectral distribution cross sections as a function of lab frame pion kinetic energy for (a) π^+, (b) π^-, (c) π^0 production from ^{4}He (400 MeV/n) + ^{12}C reactions. Plot color legends are the same as Figure 12.
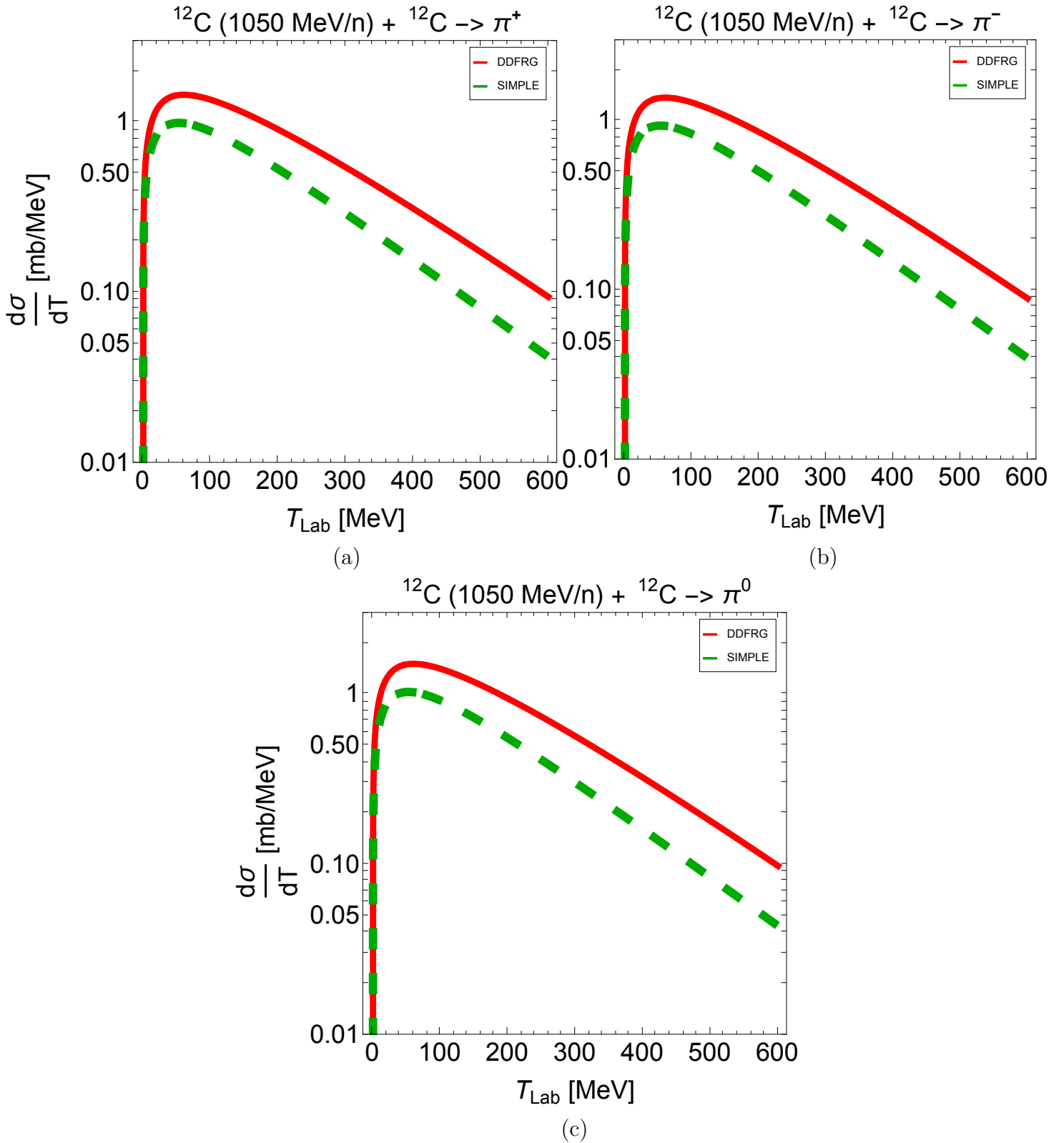
Figure 14: Spectral distribution cross sections as a function of lab frame pion kinetic energy for (a) π^+, (b) π^-, (c) π^0 production from ^{12}C (1050 MeV/n) + ^{12}C reactions. Plot color legends are the same as Figure 12.
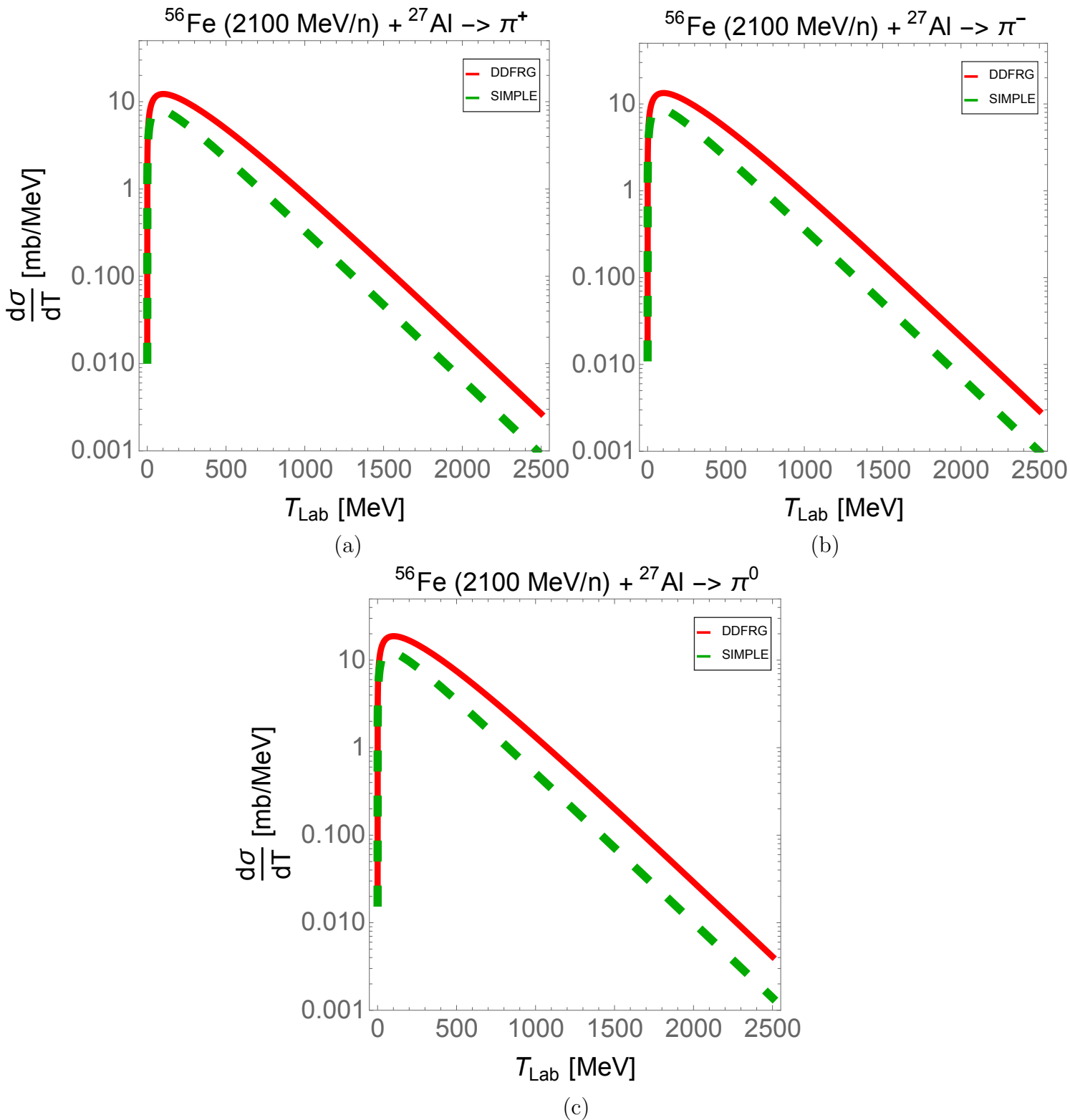
Figure 15: Spectral distribution cross sections as a function of lab frame pion kinetic energy for (a) π^+, (b) π^-, (c) π^0 production from ^{56}Fe (2100 MeV/n) + ^{27}Al reactions. Plot color legends are the same as Figure 12.

9   References

[1] S.K. Aghara, S.R. Blattnig, J.W. Norbury, R.C. Singleterry, Nucl. Inst. Meth. Phys. Res. B 267 (2009) 1115.

[2] R.B. Norman, S.R. Blattnig, G. De Angelis, F.F. Badavi, J.W. Norbury, Adv. Space Res. 50 (2012) 146.

[3] R.B. Norman, T.C. Slaba, S.R. Blattnig, Adv. Space Res. 51 (2013) 2251.

[4] T.C. Slaba, J. Wilson, C. Werneth, K. Whitman, Life Sci. Space Res. 27 (2020) 6.

[5] J.W. Norbury, Nucl. Instr. Meth. Phys. Res. A 986 (2021) 164681.

[6] J.W. Norbury, NASA Technical Publication 2020-5001740.

[7] J.W. Wilson, T.C. Slaba, F.F. Badavi, B.D. Reddell, A.A. Bahadori, Life Sci. Space Res. 2 (2014) 6.

[8] J.W. Wilson, T.C. Slaba, F.F. Badavi, B.D. Reddell, A.A. Bahadori, Life Sci. Space Res. 4 (2015) 46.

[9] J.W. Wilson, T.C. Slaba, F.F. Badavi, B.D. Reddell, A.A. Bahadori, Life Sci. Space Res. 7 (2015) 27.

[10] J.W. Wilson, T.C. Slaba, F.F. Badavi, B.D. Reddell, A.A. Bahadori, Life Sci. Space Res. 9 (2016) 69.

[11] T.C. Slaba, J.W. Wilson, F.F. Badavi, B.D. Reddell, A.A. Bahadori, Life Sci. Space Res. 9 (2016) 77.

[12] J.W. Norbury, F. Dick, NASA Technical Publication 2008-215543.

[13] C.M. Werneth, J.W. Norbury, S.R. Blattnig, Nucl. Instr. Meth. Phys. Res. B 298 (2013) 86.

[14] J.W. Norbury, NASA Technical Publication 2018-220077.

[15] M.R. Spiegel, Mathematical Handbook, Schaum's Outline Series, McGraw-Hill, New York, p. 141, 1968.

[16] J.W. Norbury, L.W. Townsend, Nucl. Instr. Meth. Phys. Res. B 254 (2007) 187.

[17] J.W. Norbury, S.R. Blattnig, R. Norman, R.K. Tripathi, NASA Technical Publication 2002-211766.

[18] J.W. Norbury, S.R. Blattnig, R.K. Tripathi, NASA Technical Publication 2002-211957.